

See discussions, stats, and author profiles for this publication at: <https://www.researchgate.net/publication/309394412>

Modeling Spacecraft Orbit–Attitude Coupled Dynamics in Close Proximity to Asteroids

Conference Paper · September 2016

DOI: 10.2514/6.2016-5204

CITATIONS

7

READS

180

2 authors:



Dante Bolatti

Ryerson University

6 PUBLICATIONS 9 CITATIONS

[SEE PROFILE](#)



Anton H. J. de Ruiter

Ryerson University

102 PUBLICATIONS 642 CITATIONS

[SEE PROFILE](#)

Some of the authors of this publication are also working on these related projects:



Improvement of disturbance rejection characteristics of the magnetic sliding mode attitude controller via disturbance observer based control method [View project](#)



DESCENT CubeSat Mission [View project](#)

Modeling Spacecraft Orbit-Attitude Coupled Dynamics in Close Proximity to Asteroids

Dante A. Bolatti* and Anton H. J. de Ruiter†

Ryerson University, Toronto, Ontario, M5B 2K3, Canada

Asteroids possess highly irregular rotating gravitational fields, and together with other destabilizing factors such as solar gravitational influence, motivates the development of precise modeling of the gravitational field and spacecraft dynamics near its surface. Typically, the spacecraft is assumed to be a point-mass, and this simplified model neglects the coupling between orbital and rotational motions of a rigid body. Additionally, in recent works that consider the spacecraft as a rigid body, a second degree-and-order spherical harmonics gravitational field has been used for the asteroid. This model does not accurately reflect the complex gravitational field of most small bodies, and does not converge inside the Brillouin sphere. This paper proposes a high fidelity gravitational model, that accounts for the orbital-attitude coupling effect for a rigid body spacecraft, while reflecting more accurately the irregular gravitational field of asteroids. This proposed model is based on the polyhedron gravitational model, augmented with point-masses distributed in the interior of the small body shape model. Simulations for the orbital motion of a rigid body spacecraft are presented, where the proposed gravitational model is compared to the spherical harmonics gravitational model expanded up to second degree-and-order. A comparison between point-mass and rigid body spacecraft orbital trajectories is also shown. These simulations are performed for trajectories in close proximity to asteroids 433 Eros and 4769 Castalia, including the gravitational effects of the Sun.

Nomenclature

\mathcal{F}	Reference frame
\mathbf{C}_{ba}	Rotation matrix that transforms vector coordinates from \mathcal{F}_a to \mathcal{F}_b
$\mathbf{E}_e, \mathbf{F}_f$	Edge and facet dyad
\mathbf{F}_g	Gravitational force [kN]
\mathbf{F}_{p_i}	Higher order gravitational force due to the i -th point-mass [kN]
\mathbf{G}_g	Gravity-gradient torque [kN km]
\mathbf{I}_s	Spacecraft second moment of inertia matrix [kg km ²]
$\mathbf{b}_a, \mathbf{b}_o$	Asteroid and spacecraft inertial position vectors (in \mathcal{F}_I) [km]
\mathbf{e}	Edge vector
\mathbf{f}_g	Higher order gravitational force term [kN]
\mathbf{g}_g	Higher order gravity gradient torque term [kN km]
\mathbf{n}	Normal vector
\mathbf{q}	Spacecraft quaternion
\mathbf{r}_{c_i}	Position vector of the i -th point-mass with respect to the asteroid's CM [km]
\mathbf{r}_e	Vector from field point to vertex of edge [km]
\mathbf{r}_f	Vector from field point to vertex of facet [km]
\mathbf{r}_{p_i}	Vector from the i -th point-mass to spacecraft's CM [km]
\mathbf{r}_s	Spacecraft's relative position vector with respect to asteroid [km]

*Graduate Student, Ryerson Aerospace Control Systems Research Group, Department of Aerospace Engineering, George Vari Engineering and Computing Centre, Student Member AIAA, dante.bolatti@ryerson.ca

†Associate Professor and Canada Research Chair in Spacecraft Dynamics and Controls, Department of Aerospace Engineering, George Vari Engineering and Computing Centre, Senior Member AIAA, aderuiter@ryerson.ca

\mathbf{v}	Vertex position vector expressed in \mathcal{F}_s [km]
C_k^j, S_k^j	Sectorial harmonics
E	Global Truncation Error (GTE)
G	Universal gravitational constant [$\text{km}^3 \text{ kg}^{-1} \text{ s}^{-2}$]
I_-	Moment of inertia scalar component for spacecraft (subscript denotes axes)
J_k	Zonal harmonics
K	Constant for calculation of GTE
L_e	Dimensionless edge factor
M	Asteroid's mass [kg]
N	Quantity of point-masses inside the asteroid's shape
O_r	Orbital radius [km]
P_k^j	Associated Legendre functions
V	Gravitational potential on a point-mass due to the asteroid [MJ kg $^{-1}$]
h	Numerical integration time-step [s]
m_s	Spacecraft mass [kg]
r_o	Normalization reference radius [km]
w, h, t	Width, height and depth of spacecraft [m]
ω_{bi}	Angular velocity between spacecraft body-fixed frame \mathcal{F}_b and inertial frame \mathcal{F}_I [rad s $^{-1}$]
ρ	Relative position vector [km]
β	Asteroid rotation axis Ecliptic latitude [°]
ε	Orbital-attitude coupling parameter
ζ	Term for Taylor expansion, defined as r_s/b_a
η_i	Mass corresponding to the i -th point-mass [kg]
θ	Field point longitude with respect to asteroid [°]
ι	Measure of spacecraft size [m]
λ	Asteroid rotation axis Ecliptic longitude [°]
μ	Gravitational parameter [$\text{km}^3 \text{ s}^{-2}$]
ρ	Polyhedron density [kg km $^{-3}$]
ϕ	Field point latitude with respect to asteroid [°]
ω_f	Dimensionless facet factor

Subscripts

$_{0,2,4}$	Denotes zeroth, second and fourth order
$_a$	Denotes quantity associated with the asteroid
$_i$	Denotes quantity associated with the i -th point-mass
$_s$	Denotes quantity associated with the Sun
$_e$	Indicates that the vector is associated with an edge
$_f$	Indicates that the vector is associated with a facet
$_{ga}$	Denotes force/torque due to the asteroid
$_{gs}$	Denotes force/torque due to the Sun
$_{po}$	Denotes Polyhedron gravitational model
$_{sh}$	Denotes Spherical Harmonics gravitational model

Superscripts

p	Indicates vector coordinates expressed in \mathcal{F}_p , corresponding to the i -th point-mass
I	Indicates vector coordinates expressed in \mathcal{F}_I
s	Indicates vector coordinates expressed in \mathcal{F}_s

I. Introduction

RECENT asteroid exploration missions by unmanned space crafts such as NASA's NEAR Shoemaker to asteroid 433 Eros,¹ JAXA's Hayabusa sample retrieval mission to asteroid 25143 Itokawa,² and NASA's Dawn mission to minor-planets 1 Ceres and 4 Vesta, have motivated advanced research on spacecraft dynamics in close proximity to highly irregular small bodies. Asteroids present weak, non-uniform rotating gravitational fields, and this together with additional perturbations, such as the Sun's gravitational influence, results in a complex dynamical environment for close proximity operations.³

Traditionally, studies of spacecraft dynamics operations near asteroids have modelled the spacecraft as a point-mass. This approach neglects an important phenomena, known as orbit-attitude coupling. Considering the spacecraft as a point-mass allows to study orbital motion decoupled from attitude motion. This is not true for a rigid body spacecraft, as coupling between the translational and rotational motions exist, becoming more important when the asteroid size is comparable to the spacecraft dimensions.^{4–6} More recently, a rigid body model has been considered for the spacecraft, while the asteroid is modelled as an oblate spheroid or a triaxial ellipsoid. Even though this approach provides a significant approximation to study the orbit-attitude coupling effect, the gravitational field model for oblate spheroids and triaxial ellipsoids (typically a second degree-and-order spherical harmonics expansion) is not suitable for capturing the complex gravitational field generated by the highly irregular shape that asteroids posses. Although the spherical harmonics expansion is highly accurate outside the circumscribing sphere (known as *Brillouin sphere*), it is well known that diverges inside this sphere, thus becoming useless for computations of trajectories in close proximity to the asteroid's surface. Non-homogeneous mass distribution inside an asteroid also presents perturbations that should be accounted for in the gravitational model, and the spherical harmonics second degree-and-order expansion used in the context of the study of coupled orbital-attitude motion does not allow to account for these perturbations in the spacecraft dynamics modeling.

With the advent of additional in-situ asteroid exploration missions and sample retrieval missions, such as JAXA's Hayabusa 2,⁷ NASA's OSIRIS-REx⁸ and the well publicized NASA's *Asteroid Retrieval Mission* (ARM),⁹ the spacecraft will be required to operate in very close proximity to the asteroid's surface, or even land on it. These types of operations demand a more accurate model of the asteroid's gravitational field to be accounted for in the spacecraft's *Attitude and Orbit Control System* (AOCS). An enhanced gravitational model will help to take advantage of the asteroid's natural dynamics to plan for specific orbital paths that allow to save fuel, therefore saving weight, or increasing the scientific operations time on the asteroid.

This paper first presents a comparison between the spherical harmonics second degree-and-order gravitational model by Misra et al.,¹⁰ and a novel expanded gravitational model based on the polyhedron model by Werner and Scheeres¹¹ and the work of Sincarsin,⁵ for a rigid body spacecraft. This new expanded polyhedron model converges both inside and outside of the Brillouin sphere, and accounts for orbit-attitude coupling of a rigid body spacecraft. Comparisons are then performed between a point-mass and a rigid body spacecraft under the polyhedron model, paying particular attention to the coupled orbit-attitude dynamics, and focusing in trajectories that cross the Brillouin sphere. Simulations are presented about asteroids 433 Eros and 4769 Castalia.

II. Background

Translational and rotational motion of spacecraft in close proximity to asteroids, with the spacecraft modelled as point-mass for orbital motion, has been covered in several studies. In particular, Scheeres,^{3,12,13} Scheeres et al.,¹⁴ Hu,¹⁵ and Kumar¹⁶ studied the motion of a particle about a rotating triaxial ellipsoid. More recently, Wang and Xu,¹⁷ expanded further this research by considering the spacecraft as a rigid body, including orbital-rotational coupling, and modeling the asteroid as an oblate spheroid. Misra and Sanyal,¹⁸ and Misra et al.,^{10,19} included the effects of the Sun's gravitational field and solar radiation pressure (SRP), considering the orbit-attitude coupled dynamics as well. In these studies, the gravitational field was modelled as a rotating spherical harmonics second degree-and-order expansion, and either an oblate spheroid or triaxial ellipsoid was used to represent the asteroid, and for computation of the sectorial harmonics C_2^0 and C_2^2 .

Other studies have used the polyhedron gravitational model developed by Werner and Scheeres¹¹ to account for perturbations due to the irregular gravitational field of an asteroid. This model allows to accurately calculate the gravitational potential for a field point outside a polyhedron shape of constant density. A work by Lantoine and Braun²⁰ uses a spherical harmonics expansion for a point-mass spacecraft, switching to the polyhedron model when inside the Brillouin sphere. Park, Werner and Bashkaran²¹ use the polyhedron model to calculate the gravitational potential of an asteroid through the sum of the polyhedron potential of cubes filling the shape (finite element approach). They also study the inverse problem, i.e. how to estimate the density of each cube assuming that "a shape model, radiometric measurements, and a priori density constraints" are known or given. An additional work by Yu and He-xi²² uses the polyhedron model to study the motion of a rover-type surface vehicle, modelled as a particle, over asteroid 1620 Geographos. None of these studies considers the spacecraft as a rigid body, therefore they do not include the effects of orbit-attitude coupling.

Another gravitational model that has been typically used is to fill the asteroid shape models with point-masses. Early studies that used point-masses for the representation of the gravitational potential were performed in 1968 by Muller and Sjogren,²³ and in 1971 by Sjogren et al.,²⁴ for the computation of a gravimetric map of the Moon for the Apollo manned missions. Recently, the need to represent gravitational potential in irregular shapes such as asteroids has brought a renewed interest in this model (Geissler et al.,²⁵ Ashenberg,²⁶ Scheeres,³ Russell²⁷). The point-masses model was used by the Hayabusa team to represent the gravitational field of asteroid 25143 Itokawa.²⁸ It has been shown by Werner and Scheeres¹¹ that despite the fact that this approach shows a good precision for the gravitational potential, the gravitational acceleration presents large errors close to the surface, due to empty spaces between point-masses. Also, producing a point-masses distribution that accurately fits the real gravitational field with its non-homogeneous mass distribution is difficult.³

As the size of the spacecraft becomes comparable to that of the asteroid, the effects of orbital-attitude coupling become significant, and can no longer be ignored for spacecraft operations in close proximity to asteroids.¹⁹ Hughes,⁶ and Sincarsin and Hughes²⁹ introduced the *orbital-attitude coupling parameter* $\varepsilon = (\iota/O_r)$, where ι is a measure of the spacecraft size, and O_r is the orbital radius. In their work, this parameter is used in the study of very large space crafts in low Earth orbit (LEO) applications ($\varepsilon \approx 10^{-4}$), but can be used as well to describe the motion of a small spacecraft about a small body, were the coupling parameter values are in the proximity of, or larger than 10^{-4} . For a rigid body, the gravitational force and torque terms on a mass element due to a point-mass can be expanded in a Taylor series on the parameter ε . Thus, higher order terms can be retained to account for the orbit-attitude coupling effect. For a typical spacecraft on LEO orbit, terms above $\mathcal{O}(\varepsilon^2)$ are discarded, but it is of interest to keep terms up to $\mathcal{O}(\varepsilon^4)$ for asteroid exploration missions.

To account for the orbit-attitude coupling effect on a rigid body spacecraft, this paper introduces an expanded polyhedron model that includes higher order terms, by considering several point-masses distributed on a uniform three dimensional grid filling the entire asteroid polyhedron shape model.

III. Asteroid Model

In this work, the asteroid shape is represented by a polyhedron with triangular facets, based on information available on NASA's Planetary Data System – Small Bodies Node (PDS-SBN).³⁰ For asteroid 433 Eros, the shape model consists of 7790 triangular facets, with 3897 vertices. Asteroid 4769 Castalia is modelled as a polyhedron with 4092 triangular facets, and 2048 vertices. Both asteroids are modelled as point-masses for their respective translational motions about the Sun, which is reasonable given the small size of the asteroid relative to its heliocentric orbital radius. To account for their rotational motions, they are considered to have constant spins about their maximum moment of inertia axes. Figure 1 shows the polyhedron model for asteroid 4769 Castalia, as implemented for simulations.

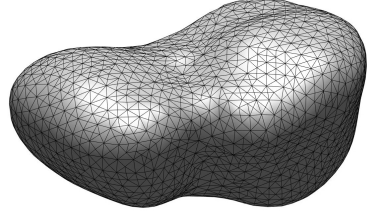


Figure 1. Polyhedron shape model for asteroid 4769 Castalia

A. Reference Frames

For the study of the asteroid and spacecraft motions, several reference frames are used, as shown in figure 2. These frames are defined as:

Inertial Frame \mathcal{F}_I : Heliocentric, where $\hat{\mathbf{x}}_I$ points in the direction of the asteroid's perihelion, $\hat{\mathbf{z}}_I$ points in the direction of the ecliptic plane North pole, and $\hat{\mathbf{y}}_I$ completes the orthogonal triad.

Asteroid body-fixed frame \mathcal{F}_s : Centered on the asteroid's center of mass, with axes $\hat{\mathbf{x}}_s$, $\hat{\mathbf{y}}_s$, and $\hat{\mathbf{z}}_s$, coincident with the asteroid's principal axes. This frame rotates with angular velocity $\vec{\omega}_{sI}$ with respect to \mathcal{F}_I .

Spacecraft body-fixed frame \mathcal{F}_b : Centered on the spacecraft's center of mass, with axes $\hat{\mathbf{x}}_b$, $\hat{\mathbf{y}}_b$, and $\hat{\mathbf{z}}_b$, coincident with the spacecraft's principal axes. This frame rotates with angular velocity $\vec{\omega}_{bI}$ with respect to \mathcal{F}_I .

Point-mass frame \mathcal{F}_{p_i} : Centered on each i -th point-mass, with axes

$$\begin{aligned}\hat{\mathbf{x}}_{p_i} &= \frac{\mathbf{r}_{p_i}}{\|\mathbf{r}_{p_i}\|} \\ \hat{\mathbf{z}}_{p_i} &= \frac{\hat{\mathbf{x}}_{p_i} \times \hat{\mathbf{x}}_I}{\|\hat{\mathbf{x}}_{p_i} \times \hat{\mathbf{x}}_I\|} \\ \hat{\mathbf{y}}_{p_i} &= \frac{\hat{\mathbf{z}}_{p_i} \times \hat{\mathbf{x}}_{p_i}}{\|\hat{\mathbf{z}}_{p_i} \times \hat{\mathbf{x}}_{p_i}\|}\end{aligned}\quad (1)$$

where \mathbf{r}_{p_i} is the vector from each point-mass to the spacecraft's center of mass, as shown in figure 2 (frames \mathcal{F}_{p_1} and \mathcal{F}_{p_2} are shown). The purpose of these axes definitions is to have the axis $\hat{\mathbf{x}}_{p_i}$ parallel to the vector \mathbf{r}_{p_i} , as this simplifies the expansion of higher order terms for the gravitational force and gravity-gradient torque.⁵ In Eq. (1), axis $\hat{\mathbf{z}}_{p_i}$ is defined with a cross product that for certain spacecraft positions may be null. If axes $\hat{\mathbf{x}}_{p_i}$ and $\hat{\mathbf{x}}_I$ are parallel, axis $\hat{\mathbf{z}}_{p_i}$ can instead be defined as $\hat{\mathbf{z}}_{p_i} = \hat{\mathbf{x}}_{p_i} \times \hat{\mathbf{y}}_I / \|\hat{\mathbf{x}}_{p_i} \times \hat{\mathbf{y}}_I\|$. There are a total of N frames.

Point-mass complementary frame \mathcal{F}_{c_i} : Centered in the spacecraft's center of mass, with axes

$$\begin{aligned}\hat{\mathbf{z}}_{c_i} &= -\hat{\mathbf{x}}_{p_i} \\ \hat{\mathbf{y}}_{c_i} &= -\hat{\mathbf{z}}_{p_i} \\ \hat{\mathbf{x}}_{c_i} &= \hat{\mathbf{y}}_{p_i}\end{aligned}\quad (2)$$

Similarly to \mathcal{F}_{p_i} , this frame is calculated for each i -th point-mass over the asteroid's surface, for a total of N frames.

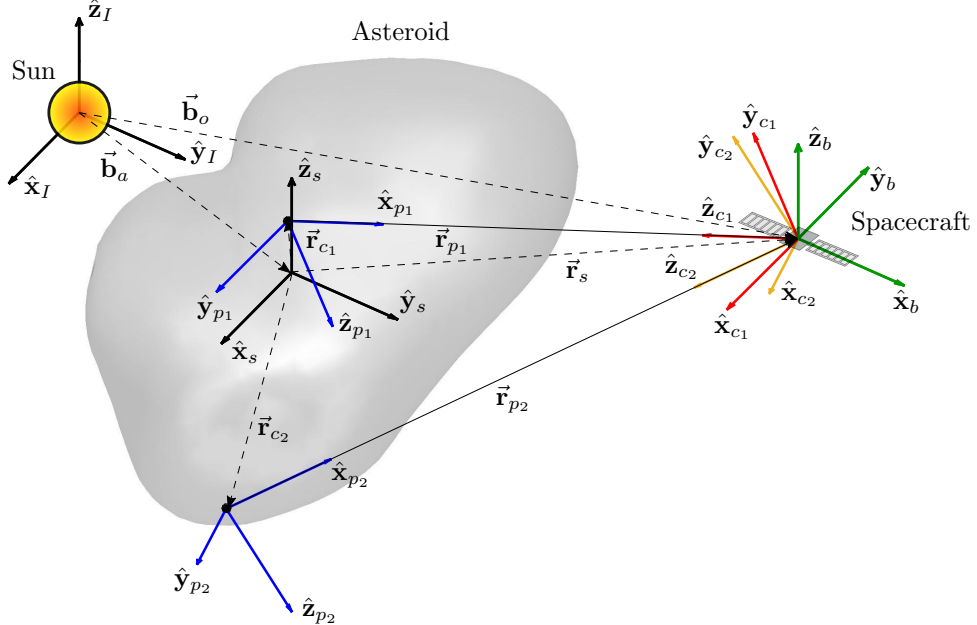


Figure 2. Reference coordinate frames for asteroid and spacecraft dynamics

B. Asteroid Equations of Motion

The asteroid attitude in the inertial frame (i.e. the orientation of body-fixed frame \mathcal{F}_s with respect to \mathcal{F}_I) can be described by a rotation matrix \mathbf{C}_{sI} , that transforms vector coordinates from the inertial frame \mathcal{F}_I to the asteroid body-fixed frame \mathcal{F}_s . For a constant spin about the $\hat{\mathbf{z}}_s$ axis, the angular velocity of frame \mathcal{F}_s with respect to \mathcal{F}_I is constant, and can be denoted by $\boldsymbol{\omega}_{sI} = [0 \ 0 \ \omega_{sz}]^T$. Hence, the evolution in time of the rotation matrix \mathbf{C}_{sI} can be calculated as the product of two rotation matrices: one that represents the

initial asteroid's attitude (namely \mathbf{C}_0); and another one that varies with time (namely \mathbf{C}_z), representing a constant time-dependent rotation about the $\hat{\mathbf{z}}_s$ axis. Therefore, asteroid kinematics can be expressed as

$$\mathbf{C}_{sI}(t) = \mathbf{C}_z(t)\mathbf{C}_0 = \begin{bmatrix} \cos(\omega_{sz}t) & \sin(\omega_{sz}t) & 0 \\ -\sin(\omega_{sz}t) & \cos(\omega_{sz}t) & 0 \\ 0 & 0 & 1 \end{bmatrix} \mathbf{C}_0 \quad (3)$$

Referring back to figure 2, and assuming that the asteroid is modelled as a point-mass for orbital motion about the Sun, with a position vector $\vec{\mathbf{b}}_a$ resolved in the inertial frame \mathcal{F}_I , the translational dynamics in the inertial frame can then be written as

$$\ddot{\mathbf{b}}_a^I = -\frac{\mu_s}{b_a^3} \mathbf{b}_a^I \quad (4)$$

where μ_s is the Sun's gravitational parameter, and $b_a = \|\mathbf{b}_a\|$.

IV. Spacecraft Model

In this study, the spacecraft is modelled both as a point-mass, and as a rigid body. The point-mass equations of motion will be presented under the polyhedron gravitational model only, as the spherical harmonics point-mass model is covered thoroughly in the cited literature. The spacecraft rigid body equations of motion will be developed for two gravitational models: the spherical harmonics model, and a proposed polyhedron augmented model. Comparisons are then presented between these three models in the numerical simulations section.

A. Point-mass Spacecraft – Equations of Motion

This is typically the model used in most studies of orbital motion about asteroids. The spacecraft is assumed to be a point-mass for the purposes of orbital dynamics calculations, with all its mass m_s concentrated in the center of mass (CM). Under the point-mass assumption, rotational motion is de-coupled from the orbital motion and can be studied separately, thus it will not be included in the following analysis.

The polyhedron gravitational model was derived in closed form by Werner and Scheeres in Ref. 11. In this model, the gravitational potential for a field point outside a constant density polyhedron shape is calculated as the contribution of each edge and facet's potential. Thus, for a given polyhedron shape of constant density, this gravity field calculation is exact.¹¹

In a polyhedron model for an asteroid, a triangular facet is specified by three vertices. An outward pointing unit normal vector $\hat{\mathbf{n}}_f$ is associated with each facet. There are three vectors associated with each facet, named \mathbf{r}_{f1} , \mathbf{r}_{f2} , and \mathbf{r}_{f3} , defined from the field point to each vertex of the facet. Each facet has three edges, and each edge e shares two facets, A and B , as shown in figure 3. An edge is associated with two vectors from the field point to each of its two vertexes (\mathbf{v}_1 and \mathbf{v}_2), namely \mathbf{r}_{e1} and \mathbf{r}_{e2} . Thus, the edge vector can be defined as $\mathbf{e} = \mathbf{r}_{e1} - \mathbf{r}_{e2}$. Corresponding to each edge, an edge normal can be defined as the unit vector that is perpendicular to both the edge e and a facet normal, pointing away from the facet center. Therefore, each edge has two normals (namely $\hat{\mathbf{n}}_e^A$ and $\hat{\mathbf{n}}_e^B$), one corresponding to each adjacent facet. With these definitions, the gravitational potential on a field point due to an asteroid modelled as a polyhedron can be defined as

$$V_{po}(\mathbf{r}_s^s) = \frac{1}{2}G\rho \sum_{e \in \text{edges}} \mathbf{r}_e^T \mathbf{E}_e \mathbf{r}_e \cdot L_e - \frac{1}{2}G\rho \sum_{f \in \text{faces}} \mathbf{r}_f^T \mathbf{F}_f \mathbf{r}_f \cdot \omega_f \quad (5)$$

where G is the universal gravitational constant, ρ is the polyhedron density, \mathbf{r}_e is a vector from the field point to any point on the edge common to two facets (e.g. \mathbf{r}_{e1}), and \mathbf{r}_f is a vector from the field point to any point on the facet (e.g. \mathbf{r}_{f1}). It is clear that these two vectors depend on $\mathbf{r}_s^s = \mathbf{C}_{sI}(\mathbf{b}_o^I - \mathbf{b}_a^I)$. The constants

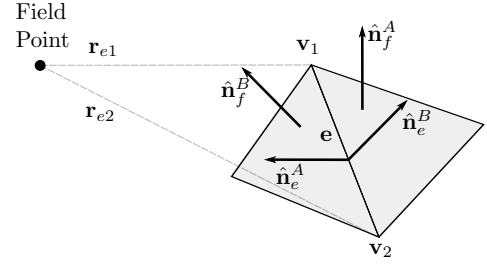


Figure 3. Polyhedron adjacent facets and edge normals

edge dyad \mathbf{E}_e and face dyad \mathbf{F}_f are defined as

$$\mathbf{E}_e = \hat{\mathbf{n}}_f^A \hat{\mathbf{n}}_e^{A^T} + \hat{\mathbf{n}}_f^B \hat{\mathbf{n}}_e^{B^T} \quad (6)$$

$$\mathbf{F}_f = \hat{\mathbf{n}}_f \hat{\mathbf{n}}_f^T \quad (7)$$

where $\hat{\mathbf{n}}_f^A$ and $\hat{\mathbf{n}}_f^B$ are the normal unity vectors of adjacent facets that share a common edge, and $\hat{\mathbf{n}}_e^A$ and $\hat{\mathbf{n}}_e^B$ are the edge normals. The dimensionless factors L_e (defined for each edge), and ω_f (defined for each facet) are calculated as

$$L_e = \ln \frac{r_{e1} + r_{e2} + e}{r_{e1} + r_{e2} - e} \quad (8)$$

$$\omega_f = 2 \arctan \frac{\mathbf{r}_{f1}^T (\mathbf{r}_{f2})^\times \mathbf{r}_{f3}}{r_{f1} r_{f2} r_{f3} + r_{f1} (\mathbf{r}_{f2}^T \mathbf{r}_{f3}) + r_{f2} (\mathbf{r}_{f3}^T \mathbf{r}_{f1}) + r_{f3} (\mathbf{r}_{f1}^T \mathbf{r}_{f2})} \quad (9)$$

where $r_f = \|\mathbf{r}_f\|$, $r_e = \|\mathbf{r}_e\|$, $e = \|\mathbf{e}\|$, and the operator $(\cdot)^\times$ transforms a vector to a *skew symmetric matrix*.

The first-order partial derivative of the gravitational potential with respect to \mathbf{r}_s^s (i.e. the gradient of Eq. (5)) is given by¹¹

$$\frac{\partial V_{po}}{\partial \mathbf{r}_s^s} = -G\rho \sum_{e \in \text{edges}} \mathbf{E}_e \mathbf{r}_e \cdot L_e + G\rho \sum_{f \in \text{faces}} \mathbf{F}_f \mathbf{r}_f \cdot \omega_f \quad (10)$$

Then, considering the gravitational influence from the Sun, and with $b_o = \|\mathbf{b}_o\|$, the acceleration of a mass-less particle can be expressed in the inertial frame as

$$\ddot{\mathbf{b}}_o^I = \frac{\partial V_s}{\partial \mathbf{b}_o^I} + \frac{\partial V_{po}}{\partial \mathbf{r}_s^s} \quad (11)$$

where referring back to figure 2, the relative position of the spacecraft with respect to the asteroid is $\mathbf{r}_s^I = \mathbf{b}_o - \mathbf{b}_a$, and where V_s represents the gravitational potential of the Sun (assumed to be a point-mass). The Sun's contribution is then expressed as

$$\frac{\partial V_s}{\partial \mathbf{b}_o^I} = -\frac{\mu_s}{b_o^3} \mathbf{b}_o^I \quad (12)$$

and the asteroid gravitational contribution resolved in \mathcal{F}_I as

$$\frac{\partial V_{po}}{\partial \mathbf{r}_s^I} = \mathbf{C}_{sI}^T \left(\frac{\partial V_{po}}{\partial \mathbf{r}_s^s} \right) \quad (13)$$

Therefore, replacing Eqs. (12) and (13) in Eq. (11), the translational dynamics of a point-mass spacecraft using the polyhedron gravitational model can be expressed as

$$\ddot{\mathbf{b}}_o^I = -\frac{\mu_s}{b_o^3} \mathbf{b}_o^I + \mathbf{C}_{sI}^T \frac{\partial V_{po}}{\partial \mathbf{r}_s^s} \quad (14)$$

The acceleration of the spacecraft relative to the asteroid is calculated as $\ddot{\mathbf{r}}_s^I = \ddot{\mathbf{b}}_o^I - \ddot{\mathbf{b}}_a^I$. Then, by using Eqs. (4) and (14), the point-mass spacecraft relative dynamics are expressed in the inertial frame \mathcal{F}_I as

$$\ddot{\mathbf{r}}_s^I = -\frac{\mu_s}{b_o^3} \mathbf{b}_o^I + \frac{\mu_s}{b_a^3} \mathbf{b}_a^I + \mathbf{C}_{sI}^T \frac{\partial V_{po}}{\partial \mathbf{r}_s^s} \quad (15)$$

It is important to note that despite the fact that this model assumes a polyhedron shape model of constant density for the asteroid, this is not a limitation of the method. A polyhedron shape can be decomposed in multiple polyhedra with different densities, similar to the finite element approach in Ref. 21. Then the asteroid contribution in Eq. (13) will become a sum of the contributions of the different polyhedra.

B. Rigid Body Spacecraft – Equations of Motion

During this study, the spacecraft is assumed to be a rectangular cuboid rigid body, with homogeneous mass distribution. No elastic deformations and no additional spacecraft devices (such as solar panels, nozzles or antennas) are assumed. Even though this is a simplified model for the purposes of numerical analysis, the method proposed in this study is general, and can be applied to any spacecraft shape. In the following sections, expressions are developed for the coupled translational-rotational dynamics, and presented together with the spacecraft kinematics for the spherical harmonics (as per Ref. 10) and the proposed expanded polyhedron models.

1. Attitude Kinematics

The spacecraft orientation with respect to the inertial frame \mathcal{F}_I can be represented by a quaternion $\mathbf{q} = [q_1 \ q_2 \ q_3 \ q_0]^T$. Considering that the spacecraft body-fixed frame \mathcal{F}_b rotates with an angular velocity $\vec{\omega}_{bI}$ with respect to the inertial frame, and resolving this angular velocity in the spacecraft body-fixed frame \mathcal{F}_b , the spacecraft kinematics can be written as

$$\dot{\mathbf{q}} = -\frac{1}{2} \begin{bmatrix} (\omega_{bI}^b)^{\times} & -\omega_{bI}^b \\ (\omega_{bI}^b)^T & 0 \end{bmatrix} \begin{bmatrix} q_1 \\ q_2 \\ q_3 \\ q_0 \end{bmatrix} \quad (16)$$

$$\mathbf{C}_{bI} = \begin{bmatrix} q_0^2 + q_1^2 - q_2^2 - q_3^2 & 2(q_1 q_2 + q_0 q_3) & 2(q_1 q_3 - q_0 q_2) \\ 2(q_1 q_2 - q_0 q_3) & q_0^2 - q_1^2 + q_2^2 - q_3^2 & 2(q_2 q_3 + q_0 q_1) \\ 2(q_1 q_3 + q_0 q_2) & 2(q_2 q_3 - q_0 q_1) & q_0^2 - q_1^2 - q_2^2 + q_3^2 \end{bmatrix} \quad (17)$$

2. Spherical Harmonics Model

The gravitational potential on a field point outside the Brillouin sphere of a body can be represented by an infinite series expansion of spherical orthogonal functions in spherical coordinates as³³

$$V_{sh}(r_s, \phi, \theta) = \frac{\mu_a}{r_s} + \frac{\mu_a}{r_s} \left[\sum_{k=2}^{\infty} \left(\frac{r_o}{r_s} \right)^k \left(-J_k P_k(\sin \phi) + \sum_{j=1}^k P_k^j(\sin \phi) (C_k^j \cos(j\theta) + S_k^j \sin(j\theta)) \right) \right] \quad (18)$$

where $r_s = \|\mathbf{r}_s\|$ is the distance from the attracting body center of mass to the field point, ϕ and θ indicate latitude and longitude of the field point, the term μ_a is the asteroid gravitational parameter, and r_o is a reference radius used for coefficient normalization (typically chosen as the Brillouin sphere radius). The coefficients J_k are known as the *zonal harmonics*, and the coefficients C_k^j and S_k^j are known as the *sectorial harmonics*. $P_k^j(\sin \phi)$ represents the *associated Legendre functions*, defined as

$$P_k^j(v) = (1 - v^2)^{\frac{1}{2}j} \frac{d^j}{dv^j}(P_k(v)) \quad (19)$$

The term $P_k(\sin \phi)$ represents the *Legendre polynomials*, and are a special case of the Legendre functions, for $j = 0$ (i.e. $P_k^0(v) \equiv P_k(v)$). These polynomials are defined as

$$P_k(v) = \frac{1}{2^k k!} \frac{d^k}{dv^k} [(v^2 - 1)^k] \quad (20)$$

Selecting the asteroid's body-fixed frame \mathcal{F}_s with axes coincident with the asteroid's principal axes, makes the gravity coefficients C_2^1 , S_2^1 and S_2^2 vanish.^{3,15} Hence, expanding Eq. (18) up to second degree and order, and transforming back to rectangular coordinates, with $\mathbf{r}_s^s = [x \ y \ z]^T$ being the spacecraft's relative position with respect to the asteroid expressed in the asteroid's body-fixed frame \mathcal{F}_s , results in

$$\begin{aligned} V_{sh}(\mathbf{r}_s^s) &= V_0 + V_2 \\ &= \underbrace{\frac{\mu_a}{r_s} - \frac{\mu_a r_o^2 C_2^0 (x^2 + y^2 - 2z^2)}{2r_s^5}}_{V_0} + \underbrace{\frac{3\mu_a r_o^2 C_2^2 (x^2 - y^2)}{r_s^5}}_{V_2} \end{aligned} \quad (21)$$

where coefficients C_2^0 and C_2^2 are the non-vanishing sectorial harmonics up to second degree and order.

First-order partial derivatives of the gravitational potential V_{sh} with respect to \mathbf{r}_s^s results in^{10,15}

$$\frac{\partial V_{sh}}{\partial x} = -\frac{\mu_a x}{r_s^3} - \frac{\mu_a r_o^2 C_2^0 x}{r_s^5} + \frac{5\mu_a r_o^2 C_2^0 x(x^2 + y^2 - 2z^2)}{2r_s^7} + \frac{6\mu_a r_o^2 C_2^2 x}{r_s^5} - \frac{15\mu_a r_o^2 C_2^2 x(x^2 - y^2)}{r_s^7} \quad (22)$$

$$\frac{\partial V_{sh}}{\partial y} = -\frac{\mu_a y}{r_s^3} - \frac{\mu_a r_o^2 C_2^0 y}{r_s^5} + \frac{5\mu_a r_o^2 C_2^0 y(x^2 + y^2 - 2z^2)}{2r_s^7} - \frac{6\mu_a r_o^2 C_2^2 y}{r_s^5} - \frac{15\mu_a r_o^2 C_2^2 y(x^2 - y^2)}{r_s^7} \quad (23)$$

$$\frac{\partial V_{sh}}{\partial z} = -\frac{\mu_a z}{r_s^3} + \frac{2\mu_a r_o^2 C_2^0 z}{r_s^5} + \frac{5\mu_a r_o^2 C_2^0 z(x^2 + y^2 - 2z^2)}{2r_s^7} - \frac{15\mu_a r_o^2 C_2^2 z(x^2 - y^2)}{r_s^7} \quad (24)$$

Equations (22), (23), and (24) can be re-written in compact form as

$$\frac{\partial V_{sh}}{\partial \mathbf{r}_s^s} = \frac{\partial V_0}{\partial \mathbf{r}_s^s} + \frac{\partial V_2}{\partial \mathbf{r}_s^s} \quad (25)$$

For the spacecraft rigid body model, translational dynamics can be expressed as the sum of two contributions: one due to the gravitational attraction of the Sun, and another due to the asteroid. Hence, in \mathcal{F}_I we have

$$m_s \ddot{\mathbf{b}}_o^I = \mathbf{F}_{gs}^I + \mathbf{F}_{ga}^I \quad (26)$$

where m_s is the spacecraft's mass.

For the orbital motion about the Sun, the spacecraft is modelled as a point-mass, as the distance and gravitational force of the Sun acting on the spacecraft makes the orbit-attitude coupling due to the Sun negligible. Therefore

$$\mathbf{F}_{gs}^I = -m_s \frac{\mu_a}{b_o^3} \mathbf{b}_o^I \quad (27)$$

In Ref. 10, the gravitational force \mathbf{F}_{ga} due to the asteroid is calculated as the sum of two terms: a zeroth order term \mathbf{F}_{ga0} , and a second order term \mathbf{F}_{ga2} . The principal force term \mathbf{F}_{ga0} is calculated as the integral over the rigid body of the first term in the right side of Eq. (25) (i.e. the integral of the first column of Eqs. (22), (23), and (24)) retaining terms up to r_s^{-4} in the integration, while the second degree-and-order term is approximated by a force acting on the center of mass of the spacecraft (i.e. spacecraft modelled as a point-mass). Therefore, the gravitational force \mathbf{F}_{ga} can be stated on the inertial frame \mathcal{F}_I as

$$\mathbf{F}_{ga}^I = -\left(\frac{m_s \mu_a}{r_s^3}\right) \mathbf{r}_s^I - 3\left(\frac{\mu_a}{r_s^5}\right) \mathbf{I} \mathbf{r}_s^I + \frac{15}{2} \left(\frac{\mu_a ((\mathbf{r}_s^I)^T \mathbf{I}_s^I (\mathbf{r}_s^I))}{r_s^7}\right) \mathbf{r}_s^I + \mathbf{C}_{sI}^T \mathbf{F}_{ga2}^s \quad (28)$$

where

$$\mathbf{I} = (\mathbf{C}_{bI})^T \left(\frac{1}{2} \text{tr}(\mathbf{I}_s) \mathbf{1} + \mathbf{I}_s\right) (\mathbf{C}_{bI}) \quad (29)$$

$$\mathbf{I}_s^I = (\mathbf{C}_{bI})^T \mathbf{I}_s (\mathbf{C}_{bI}) \quad (30)$$

The matrix \mathbf{I}_s is the spacecraft's second order moment of inertia matrix, and \mathbf{I}_s^I represents this same matrix expressed in the inertial frame \mathcal{F}_I . By using Eqs. (22), (23) and (24), the second degree-and-order force term \mathbf{F}_{ga2}^s can be written in component form as

$$F_{ga2x}^s = m_s \left[-\left(\frac{\mu_a r_o^2 C_2^0 x}{r_s^5}\right) + \frac{5\mu_a r_o^2 C_2^0 x(x^2 + y^2 - 2z^2)}{2r_s^7} + \frac{6\mu_a r_o^2 C_2^2 x}{r_s^5} - \frac{15\mu_a r_o^2 C_2^2 x(x^2 - y^2)}{r_s^7} \right] \quad (31)$$

$$F_{ga2y}^s = m_s \left[-\left(\frac{\mu_a r_o^2 C_2^0 y}{r_s^5}\right) + \frac{5\mu_a r_o^2 C_2^0 y(x^2 + y^2 - 2z^2)}{2r_s^7} - \frac{6\mu_a r_o^2 C_2^2 y}{r_s^5} - \frac{15\mu_a r_o^2 C_2^2 y(x^2 - y^2)}{r_s^7} \right] \quad (32)$$

$$F_{ga2z}^s = m_s \left[\left(\frac{2\mu_a r_o^2 C_2^0 z}{r_s^5}\right) + \frac{5\mu_a r_o^2 C_2^0 z(x^2 + y^2 - 2z^2)}{2r_s^7} - \frac{15\mu_a r_o^2 C_2^2 z(x^2 - y^2)}{r_s^7} \right] \quad (33)$$

Hence, using Eqs. (27) and (28), the translational dynamics for a rigid body spacecraft about an asteroid can be expressed in complete form as

$$m_s \ddot{\mathbf{b}}_o^I = -m_s \frac{\mu_a}{b_o^3} \mathbf{b}_o^I - \left(\frac{m_s \mu_a}{r_s^3}\right) \mathbf{r}_s^I - 3\left(\frac{\mu_a}{r_s^5}\right) \mathbf{I} \mathbf{r}_s^I + \frac{15}{2} \left(\frac{\mu_a ((\mathbf{r}_s^I)^T \mathbf{I}_s^I (\mathbf{r}_s^I))}{r_s^7}\right) \mathbf{r}_s^I + \mathbf{C}_{sI}^T \mathbf{F}_{ga2}^s \quad (34)$$

The spacecraft relative translational dynamics with respect to the asteroid can be calculated with the help of Eqs. (4) and (34), as was similarly done for the point-mass spacecraft model, resulting in

$$m_s \ddot{\mathbf{r}}_s^I = -m_s \frac{\mu_s}{b_o^3} \mathbf{b}_o^I + m_s \frac{\mu_s}{b_a^3} \mathbf{b}_a^I - \left(\frac{m_s \mu_a}{r_s^3} \right) \mathbf{r}_s^I - 3 \left(\frac{\mu_a}{r_s^5} \right) \boldsymbol{\mathcal{I}} \mathbf{r}_s^I + \frac{15}{2} \left(\frac{\mu_a ((\mathbf{r}_s^I)^T \mathbf{I}_s^I (\mathbf{r}_s^I))}{r_s^7} \right) \mathbf{r}_s^I + \mathbf{C}_{sI}^T \mathbf{F}_{ga2}^s \quad (35)$$

Rotational dynamics of the rigid body spacecraft can be expressed in the spacecraft's body-fixed frame \mathcal{F}_b as^{4, 19, 33}

$$\mathbf{I}_s \dot{\boldsymbol{\omega}}_{bI}^b = (\mathbf{I}_s \boldsymbol{\omega}_{bI}^b)^\times \boldsymbol{\omega}_{bI}^b + \mathbf{G}_{ga}^b \quad (36)$$

where the gravity-gradient torque due to the asteroid can be expressed as

$$\mathbf{G}_{ga}^b = 3 \left(\frac{\mu_a}{r_s^5} \right) \left((\mathbf{r}_s^b)^\times \mathbf{I}_s (\mathbf{r}_s^b) \right) \quad (37)$$

with $\mathbf{r}_s^b = \mathbf{C}_{bI} \mathbf{r}_s^I$ being the spacecraft's relative position with respect to the asteroid, expressed in the spacecraft's body-fixed frame.

Equation (28) includes gravitational force terms up to the second order, assuming that all the asteroid mass is concentrated in its center of mass. The asteroid mass distribution is considered by the spherical harmonic distribution, expanded up to second-degree-and-order, via the sectorial harmonics. However, the spacecraft gravity-gradient torque expressed in Eq. (37) is also of second order, completely neglecting the mass distribution of the asteroid for the gravity gradient torque calculation. This is the gravity-gradient expression used in Ref. 10, and is also the term that is typically retained in studies of orbit-attitude coupling.²⁹ Hence, spacecraft dynamics shown in Eqs. (34) and (36) only capture orbit-attitude coupling terms of the first order. For close proximity operations to asteroids, a typical coupling parameter value ε can have a high value. Assuming $\iota = 10$ m (typical spacecraft size, including solar panels), and an orbital radius $O_r = 0.5$ km, the coupling parameter results in $\varepsilon_a = 0.02$, thus $\varepsilon_a^2 = 4 \times 10^{-4}$ and $\varepsilon_a^4 = 0.16 \times 10^{-6}$. Although these values may seem low, in a typical LEO application, assuming the same 10 m spacecraft orbiting in a 1000 km orbit (with an Earth equatorial radius of 6378 km), the coupling parameter results in $\varepsilon_e = 1.35 \times 10^{-6}$. This is comparable to ε_a^4 in an asteroid application. Therefore, this stimulates the inclusion of coupling terms up to $\mathcal{O}(\varepsilon^4)$ in the gravitational force and torque expansions. For the coupling parameters values presented, it is safe then not include terms beyond $\mathcal{O}(\varepsilon^4)$, as their contribution will be very small, while their calculation grows dramatically in complexity.⁶ A figure showing the position difference between a rigid body model considering terms up to $\mathcal{O}(\varepsilon^2)$, and the same model with terms up to $\mathcal{O}(\varepsilon^4)$ will be presented during the numerical simulations section.

An argument can be made at this point about expanding further the gravitational force in Eq. (28) to include higher order terms, therefore accounting for higher order coupling. While this method has been widely used for computing gravitational fields for oblate spheroids, it is somewhat difficult to capture the complex shape presented by asteroids by assuming spherical harmonics expansions. Also, the spherical harmonics series does not converge inside the Brillouin sphere.^{3, 4} Due to these reasons, in the following section a new gravitational model that includes second order coupling terms while capturing the complexity of the asteroid shape is developed.

3. Expanded Polyhedron Model

In Ref. 5, Sincarsin expands the gravitational force due to a point-mass to retain terms up to $\mathcal{O}(\varepsilon^4)$ to study orbit-attitude coupling of a very large spacecraft in Earth's orbit. This same approach can be used to analyze orbit-attitude coupling for a small spacecraft operating in close proximity of a small body (such as an asteroid), by distributing point-masses in its entire volume to account for the higher order coupling terms. Together with the polyhedron gravitational acceleration, this point-mass distribution allows to develop a precise gravitational field model, that faithfully represents the complex asteroid shape while including the coupling effect, and that converges for any point outside the asteroid shape. With these comments, a new gravitational field model is introduced as follows.

First, for a symmetric spacecraft, expanding the gravitational force on a rigid body due to a single point-mass up to the fourth order about ε results in^{5, 29}

$$\mathbf{F}_{pm} = \mathbf{f}_{g0} + \mathbf{f}_{g2} + \mathbf{f}_{g4} \quad (38)$$

where each term represents the contribution of zeroth order ($\mathcal{O}(\varepsilon^0)$), second order ($\mathcal{O}(\varepsilon^2)$) and fourth order ($\mathcal{O}(\varepsilon^4)$) correspondingly. Then, filling the asteroid shape with N point-masses, the resulting gravitational force on the point-mass spacecraft can be written as a summation of all the asteroid point-masses contributions, this is

$$\mathbf{F}_{pms} = \sum_{i=1}^N \mathbf{f}_{g0_i} + \sum_{i=1}^N (\mathbf{f}_{g2_i} + \mathbf{f}_{g4_i}) \quad (39)$$

The first term in Eq. (39) is the gravitational force one would get for a point-mass spacecraft influenced by an asteroid modeled by point-masses. To improve the model fidelity, we replace this term with the gravitational force resulting from a polyhedron acting on a point-mass spacecraft. Proceeding this way, we effectively improve the $\mathcal{O}(\varepsilon^0)$ term accuracy, while still capturing the asteroid mass distribution and orbit-attitude coupling effect via the higher order terms $\mathcal{O}(\varepsilon^2)$ and $\mathcal{O}(\varepsilon^4)$.

Therefore, placing N point-masses in a uniform grid inside the polyhedron shape model as shown in figure 4, the gravitational force on a rigid body spacecraft due to the asteroid can be expressed in \mathcal{F}_I as

$$\begin{aligned} \mathbf{F}_{ga}^I &= \mathbf{F}_{po}^I + \sum_{i=1}^N \mathbf{F}_{p_i}^I \\ &= m_s \frac{\partial V_{po}}{\partial \mathbf{r}_s^I} + \sum_{i=1}^N (\mathbf{f}_{g2_i}^I + \mathbf{f}_{g4_i}^I) \\ &= m_s \mathbf{C}_{SI}^T \frac{\partial V_{po}}{\partial \mathbf{r}_s^s} + \sum_{i=1}^N (\mathbf{f}_{g2_i}^I + \mathbf{f}_{g4_i}^I) \end{aligned} \quad (40)$$

where $\partial V_{po}/\partial \mathbf{r}_s^s$ is the first-order partial derivative of the polyhedron potential with respect to \mathbf{r}_s^s as shown in Eq. (10) (specific force), and the terms $\mathbf{f}_{g2_i}^I$ and $\mathbf{f}_{g4_i}^I$ are the higher order gravitational force contributions resolved in \mathcal{F}_I . When the spacecraft is modelled as a point-mass, the second term in Eq. (40) vanishes. Therefore, the summation on the second term includes the effect of attitude on the orbit, while also accounting for the asteroid mass distribution due to the point-masses distributed inside the asteroid's shape.

For the gravitational torque analysis, the higher order terms $\mathcal{O}(\varepsilon^2)$ and $\mathcal{O}(\varepsilon^4)$ are also kept, with the term $\mathcal{O}(\varepsilon^2)$ being the typical term kept for gravity-gradient torque analysis (as depicted in Eq. (37)). Then, assuming that no control torque is present, the only acting torque on the spacecraft is the gravity-gradient torque. This can be expressed for the proposed model as

$$\mathbf{G}_{ga}^b = \sum_{i=1}^N (\mathbf{g}_{g2_i}^b + \mathbf{g}_{g4_i}^b) \quad (41)$$

where again N is the total amount of point-masses distributed on the polyhedron shape model, and the torques $\mathbf{g}_{g2_i}^b$ and $\mathbf{g}_{g4_i}^b$ are the second and fourth order torque terms due to the i -th point-mass, resolved in the spacecraft body-fixed frame.

The definitions for the higher order terms of both \mathbf{F}_{ga}^I and \mathbf{G}_{ga}^b are developed specifically for the shape of the spacecraft. As in Ref. 5, the shape of the spacecraft selected for this study is a triaxial rectangular cuboid, with sizes $w \times h \times t$ (i.e. width \times height \times depth), as presented in figure 5. For this rigid body, higher order inertia terms are used to express the higher order force and torque terms, as developed by Sincarsin.⁵ For a cuboid shape, second and fourth order inertia terms are required. The second order inertia terms in component form follows the classic expressions for a cube. The fourth order inertia terms expressions,

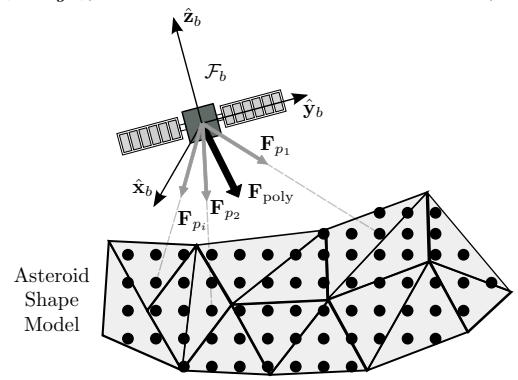


Figure 4. Proposed gravitational model

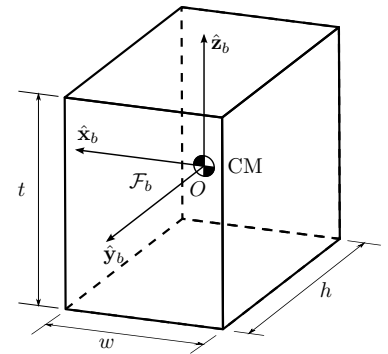


Figure 5. Triaxial rectangular cuboid spacecraft model

and their derivations can be found in Ref. 5. In the body-fixed frame \mathcal{F}_b , the inertia scalar components are therefore expressed as

$$I_{xx} = \frac{m_s}{12} (h^2 + t^2) \quad (42)$$

$$I_{yy} = \frac{m_s}{12} (w^2 + t^2) \quad (43)$$

$$I_{zz} = \frac{m_s}{12} (w^2 + h^2) \quad (44)$$

$$I_{xxxx} = \frac{m_s}{80} (h^4 + t^4) + \frac{m_s}{72} (h^2 t^2) \quad (45)$$

$$I_{xxyy} = \frac{m_s}{80} (h^4 + t^4 - w^4) + \frac{m_s}{144} h^2 (w^2 + 2t^2) \quad (46)$$

$$I_{xxzz} = \frac{m_s}{80} (h^4 + t^4 - w^4) + \frac{m_s}{144} t^2 (w^2 + 2h^2) \quad (47)$$

$$I_{yyxx} = \frac{m_s}{80} (w^4 + t^4 - h^4) + \frac{m_s}{144} w^2 (h^2 + 2t^2) \quad (48)$$

$$I_{yyyy} = \frac{m_s}{80} (w^4 + t^4) + \frac{m_s}{72} (w^2 t^2) \quad (49)$$

$$I_{yyzz} = \frac{m_s}{80} (w^4 + t^4 - h^4) + \frac{m_s}{144} t^2 (h^2 + 2w^2) \quad (50)$$

$$I_{zzxx} = \frac{m_s}{80} (w^4 + h^4 - t^4) + \frac{m_s}{144} w^2 (t^2 + 2h^2) \quad (51)$$

$$I_{zzyy} = \frac{m_s}{80} (w^4 + h^4 - t^4) + \frac{m_s}{144} h^2 (t^2 + 2w^2) \quad (52)$$

$$I_{zzzz} = \frac{m_s}{80} (w^4 + h^4) + \frac{m_s}{72} (w^2 h^2) \quad (53)$$

$$I_{xyyx} = I_{xyxy} = I_{yxxz} = I_{yxyx} = \frac{m_s}{144} w^2 h^2 \quad (54)$$

$$I_{xzzx} = I_{xzxz} = I_{zxxz} = I_{zxzx} = \frac{m_s}{144} w^2 t^2 \quad (55)$$

$$I_{yzyy} = I_{yzyz} = I_{zyyz} = I_{zyzy} = \frac{m_s}{144} h^2 t^2 \quad (56)$$

Then, as in the spherical harmonics model, the spacecraft translational dynamics can be expressed in the form of Eq. (26), this is

$$m_s \ddot{\mathbf{b}}_o^I = \mathbf{F}_{gs}^I + \mathbf{F}_{ga}^I \quad (57)$$

where the gravitational force acting on the spacecraft due to the sun \mathbf{F}_{gs} is shown in Eq. (27).

The gravitational force \mathbf{F}_{ga} due to the asteroid can then be expressed as in Eq. (40), or with the help of Sincarsin's notation in Ref. 5

$$\mathbf{F}_{ga}^I = m_s \mathbf{C}_{sI}^T \frac{\partial V_{po}}{\partial \mathbf{r}_s^s} + \sum_{i=1}^N \mathbf{C}_{Ip_i} (\mathbf{f}_{g2_i}^p + \mathbf{f}_{g4_i}^p) \quad (58)$$

where the higher order terms are expressed in the point-mass frame corresponding to the i -th point-mass, and \mathbf{C}_{Ip_i} is the rotation matrix that transforms a vector from the i -th point-mass frame \mathcal{F}_{p_i} to the inertial frame \mathcal{F}_I . This matrix can be formed for each point-mass as

$$\mathbf{C}_{Ip_i} = \begin{bmatrix} x_{p_{x,i}} & y_{p_{x,i}} & z_{p_{x,i}} \\ x_{p_{y,i}} & y_{p_{y,i}} & z_{p_{y,i}} \\ x_{p_{z,i}} & y_{p_{z,i}} & z_{p_{z,i}} \end{bmatrix} \quad (59)$$

where the matrix components are the components of each unit vector representing the axes of the frame \mathcal{F}_{p_i} , as defined in Eq. (1). Then, the force components $\mathbf{f}_{g2_i}^p$ and $\mathbf{f}_{g4_i}^p$ acting on the triaxial cuboid spacecraft due to each i -th point-mass can be stated as⁵

$$f_{g2_{ix}}^p = 3 \frac{\mu_i}{r_{p_i}^4} \left\{ \left[I_{zz} - \frac{1}{2} (I_{xx} + I_{yy}) \right] + \frac{3}{2} \left[(I_{xx} - I_{zz}) c_{13_i}^{bc^2} + (I_{yy} - I_{zz}) c_{23_i}^{bc^2} \right] \right\} \quad (60)$$

$$f_{g2_{iy}}^p = 3 \frac{\mu_i}{r_{p_i}^4} \left\{ [(I_{zz} - I_{xx}) c_{31_i}^{bc} c_{33_i}^{bc}] + [(I_{yy} - I_{xx}) c_{21_i}^{bc} c_{23_i}^{bc}] \right\} \quad (61)$$

$$f_{g2_{iz}}^p = 3 \frac{\mu_i}{r_{p_i}^4} \left\{ [(I_{yy} - I_{zz}) c_{32_i}^{bc} c_{33_i}^{bc}] + [(I_{yy} - I_{xx}) c_{12_i}^{bc} c_{13_i}^{bc}] \right\} \quad (62)$$

$$\begin{aligned} f_{g4_{ix}}^p = \frac{5}{2} \frac{\mu_i}{r_{p_i}^6} & \left\{ \frac{1}{4} \left[(\Gamma_3 - 4(\Gamma_1 + \Gamma_2)) + 35 \left\{ \left[(\Gamma_1 - \Gamma_3) + \Gamma_2 (1 - c_{13_i}^{bc^2}) \right] c_{13_i}^{bc^2} + \right. \right. \right. \right. \\ & \left. \left. \left. \left. + \left[(\Gamma_2 - \Gamma_3) + \Gamma_1 (1 - c_{23_i}^{bc^2}) \right] c_{23_i}^{bc^2} - (\Gamma_1 + \Gamma_2 - \Gamma_3) c_{13_i}^{bc^2} c_{23_i}^{bc^2} \right] \right\} \right\} \end{aligned} \quad (63)$$

$$\begin{aligned} f_{g4_{iy}}^p = \frac{5}{2} \frac{\mu_i}{r_{p_i}^6} & \left\{ \left[\{4\Xi_{cx} - 7\Xi_{bx} - 11\Xi_{dy}\} c_{31_i}^{bc} c_{33_i}^{bc} - \right. \right. \\ & \left. \left. - 7 \left\{ (\Xi_{bx} c_{13_i}^{bc} c_{11_i}^{bc} + 3\Xi_{dy} c_{23_i}^{bc} c_{21_i}^{bc} - \Xi_{ax} c_{31_i}^{bc} c_{33_i}^{bc}) c_{13_i}^{bc^2} + \Gamma_4 c_{23_i}^{bc} c_{21_i}^{bc} + \right. \right. \right. \\ & \left. \left. \left. + (3\Xi_{dx} c_{13_i}^{bc} c_{11_i}^{bc} + \Xi_{by} c_{23_i}^{bc} c_{21_i}^{bc} - \Xi_{ay} c_{31_i}^{bc} c_{33_i}^{bc}) c_{23_i}^{bc^2} \right\} \right] \right\} \end{aligned} \quad (64)$$

$$\begin{aligned} f_{g4_{iz}}^p = -\frac{5}{2} \frac{\mu_i}{r_{p_i}^6} & \left\{ \left[\{4\Xi_{cy} - 7\Xi_{by} - 11\Xi_{dx}\} c_{32_i}^{bc} c_{33_i}^{bc} - \right. \right. \\ & \left. \left. - 7 \left\{ (\Xi_{by} c_{23_i}^{bc} c_{22_i}^{bc} + 3\Xi_{dx} c_{13_i}^{bc} c_{12_i}^{bc} - \Xi_{ay} c_{32_i}^{bc} c_{33_i}^{bc}) c_{23_i}^{bc^2} - \Gamma_4 c_{13_i}^{bc} c_{12_i}^{bc} + \right. \right. \right. \\ & \left. \left. \left. + (3\Xi_{dy} c_{23_i}^{bc} c_{22_i}^{bc} + \Xi_{bx} c_{13_i}^{bc} c_{12_i}^{bc} - \Xi_{ax} c_{32_i}^{bc} c_{33_i}^{bc}) c_{13_i}^{bc^2} \right\} \right] \right\} \end{aligned} \quad (65)$$

where $\mu_i = G\eta_i$ is the i -th gravitational parameter, associated with the i -th point-mass, with mass $\eta_i = M/N$, and r_{p_i} is the distance from the the i -th point-mass to the spacecraft's center of mass. This distance can be calculated as $r_{p_i} = \|\mathbf{r}_{p_i}\| = \|\mathbf{r}_s^s - \mathbf{r}_{c_i}^s\|$, being $\mathbf{r}_{c_i}^s$ the position of each i -th point-mass, expressed in the asteroid frame \mathcal{F}_s , as defined in figure 2. The above expressions include the grouping terms Ξ_{ki} (where $k = a, b, c, d$, and $i = x, y$), and Γ_j (where $j = 1, 2, 3, 4$), that are defined as

$$\begin{aligned} \Xi_{ai} &= I_{zzzz} - 2I_{izzi} - I_{zzi} & \Gamma_1 &= I_{xxxx} - 8I_{yzyy} \\ \Xi_{bi} &= I_{iiii} - 2I_{izzi} - I_{iizz} & \Gamma_2 &= I_{yyyy} - 8I_{xzxz} \\ \Xi_{ci} &= I_{zzzz} - I_{iiii} & \Gamma_3 &= I_{zzzz} - 8I_{xyyx} \\ \Xi_{di} &= I_{xyyx} - I_{izzi} & \Gamma_4 &= \frac{11}{7} (I_{xxxx} - I_{yyyy}) + \frac{3}{7} (I_{yzyy} - I_{xzxz}) \\ & & & + (I_{yyzz} - I_{xxzz}) \end{aligned} \quad (66)$$

and the terms $c_{lm_i}^{bc}$ ($l = 1, 2, 3$ and $m = 1, 2, 3$), that are the components of the rotation matrix \mathbf{C}_{bc_i} that transforms coordinates in point-mass complementary frame \mathcal{F}_{c_i} (corresponding to the i -th point-mass) to the spacecraft's body frame \mathcal{F}_b . Referring back to figure 2, there are N rotation matrices \mathbf{C}_{bc_i} , each one defined as

$$\mathbf{C}_{bc_i} = \begin{bmatrix} \hat{\mathbf{x}}_b \cdot \hat{\mathbf{x}}_{c_i} & \hat{\mathbf{x}}_b \cdot \hat{\mathbf{y}}_{c_i} & \hat{\mathbf{x}}_b \cdot \hat{\mathbf{z}}_{c_i} \\ \hat{\mathbf{y}}_b \cdot \hat{\mathbf{x}}_{c_i} & \hat{\mathbf{y}}_b \cdot \hat{\mathbf{y}}_{c_i} & \hat{\mathbf{y}}_b \cdot \hat{\mathbf{z}}_{c_i} \\ \hat{\mathbf{z}}_b \cdot \hat{\mathbf{x}}_{c_i} & \hat{\mathbf{z}}_b \cdot \hat{\mathbf{y}}_{c_i} & \hat{\mathbf{z}}_b \cdot \hat{\mathbf{z}}_{c_i} \end{bmatrix} = \begin{bmatrix} c_{11_i}^{bc} & c_{12_i}^{bc} & c_{13_i}^{bc} \\ c_{21_i}^{bc} & c_{22_i}^{bc} & c_{23_i}^{bc} \\ c_{31_i}^{bc} & c_{32_i}^{bc} & c_{33_i}^{bc} \end{bmatrix} \quad (67)$$

where the matrix components are the dot products between the basis vectors of \mathcal{F}_b and \mathcal{F}_{c_i} .

As previously done for the spacecraft rigid body model under the spherical harmonics gravitational model, relative translational dynamics can be written using Eqs. (4) and (57) as

$$\ddot{\mathbf{r}}_s^I = -\frac{\mu_s}{b_o^3} \mathbf{b}_o^I + \frac{\mu_s}{b_a^3} \mathbf{b}_a^I + \mathbf{C}_{sI}^T \frac{\partial V_{po}}{\partial \mathbf{r}_s^s} + \frac{1}{m_s} \left(\sum_{i=1}^N \mathbf{C}_{Ip_i} (\mathbf{f}_{g2_i}^p + \mathbf{f}_{g4_i}^p) \right) \quad (68)$$

In a similar fashion, and using Eq. (41), the spacecraft rotational dynamics under this model can be expressed in the spacecraft body-fixed frame \mathcal{F}_b as

$$\begin{aligned}\mathbf{I}_s \dot{\boldsymbol{\omega}}_{bI}^b &= (\mathbf{I}_s \boldsymbol{\omega}_{bI}^b)^\times \boldsymbol{\omega}_{bI}^b + \mathbf{G}_{ga}^b \\ &= (\mathbf{I}_s \boldsymbol{\omega}_{bI}^b)^\times \boldsymbol{\omega}_{bI}^b + \sum_{i=1}^N (\mathbf{g}_{g2_i}^b + \mathbf{g}_{g4_i}^b)\end{aligned}\quad (69)$$

Here, the second and fourth order gravitational torque terms acting on the spacecraft due to the i -th point-mass can be stated as⁵

$$g_{g2_{ix}}^b = 3 \frac{\mu_i}{r_{p_i}^3} [(I_{zz} - I_{yy}) c_{23_i}^{bc} c_{33_i}^{bc}] \quad (70)$$

$$g_{g2_{iy}}^b = 3 \frac{\mu_i}{r_{p_i}^3} [(I_{xx} - I_{zz}) c_{13_i}^{bc} c_{33_i}^{bc}] \quad (71)$$

$$g_{g2_{iz}}^b = 3 \frac{\mu_i}{r_{p_i}^3} [(I_{yy} - I_{xx}) c_{13_i}^{bc} c_{23_i}^{bc}] \quad (72)$$

$$g_{g4_{ix}}^b = \frac{5}{2} \frac{\mu_i}{r_{p_i}^5} \left\{ \left[\{4\Xi_{cy} - 7\Xi_{by} - 11\Xi_{dx}\} + 7 \left\{ (\Xi_{ax} + 3\Xi_{dy}) c_{13_i}^{bc^2} + (\Xi_{ay} + \Xi_{by}) c_{23_i}^{bc^2} \right\} \right] c_{23_i}^{bc} c_{33_i}^{bc} \right\} \quad (73)$$

$$g_{g4_{iy}}^b = -\frac{5}{2} \frac{\mu_i}{r_{p_i}^5} \left\{ \left[\{4\Xi_{cx} - 7\Xi_{bx} - 11\Xi_{dy}\} + 7 \left\{ (\Xi_{ay} + 3\Xi_{dx}) c_{23_i}^{bc^2} + (\Xi_{ax} + \Xi_{bx}) c_{13_i}^{bc^2} \right\} \right] c_{13_i}^{bc} c_{33_i}^{bc} \right\} \quad (74)$$

$$g_{g4_{iz}}^b = \frac{5}{2} \frac{\mu_i}{r_{p_i}^5} \left\{ \left[\left\{ -7\Gamma_4 - 7 \left[(3\Xi_{dy} - \Xi_{bx}) c_{13_i}^{bc^2} - (3\Xi_{dx} - \Xi_{by}) c_{23_i}^{bc^2} \right] \right\} \right] c_{13_i}^{bc} c_{23_i}^{bc} \right\} \quad (75)$$

Once again the grouping terms defined in Eq. (66), and the coefficients of the rotation matrix \mathbf{C}_{bc_i} defined in Eq. (67) are used.

V. Numerical Simulations

A. Implementation considerations

In this paper, the equations of motion are directly discretized with respect to time, so they can be integrated via the Runge-Kutta method. The spacecraft quaternions \mathbf{q} are renormalized at each integration step, to keep the norm error close to machine precision.

A closer look at the spacecraft relative translational dynamics for the three models (Eqs. (15), (35), and (68)) shows that the first two terms present a subtraction of two nearly equal numbers, due to \mathbf{b}_o^I being very close in value to \mathbf{b}_a^I (this can be seen in figure 2). When computing this operation in a double-precision processor, using floating-point arithmetic (as is the usual case for numerical integration), these two terms produce a *catastrophic cancellation*, inducing an effect that is known as *loss of significance* (LOS). This results in a loss of accurate digits in the solution, therefore reducing numerical accuracy to unacceptable levels during integration. Since the relative dynamics between the spacecraft and asteroid are the values of interest, in order to avoid the LOS effect, a similar approach to the one used to study the relative motion equation in spacecraft formation flying is used.³³ This method requires the Sun's contribution to be rewritten as a function of $\mathbf{b}_a^I + \mathbf{r}_s^I$. Thus, expanding this term

$$-\frac{\mu_s}{b_o^3} \mathbf{b}_o^I = -\mu_s \frac{(\mathbf{b}_a^I + \mathbf{r}_s^I)}{\|\mathbf{b}_a^I + \mathbf{r}_s^I\|^3} \quad (76)$$

Expanding the denominator of Eq. (76), defining $\zeta \triangleq (r_s/b_a)$, and approximating via a Taylor series to the first order around ζ , the Sun's contribution can be approximated as

$$-\frac{\mu_s}{b_o^3} \mathbf{b}_o^I \approx -\frac{\mu_s}{b_a^3} (\mathbf{b}_a^I + \mathbf{r}_s^I) \left(1 - \frac{3(\mathbf{r}_s^I)^T \mathbf{b}_a^I}{b_a^2} \right) \quad (77)$$

Substituting Eq. (77) in Eqs. (15), (35) and (68), we approximate the spacecraft relative dynamics for numerical simulation on each gravitational model as

- Point-mass spacecraft relative dynamics under polyhedron model gravitation,

$$\ddot{\mathbf{r}}_s^I \approx -\frac{\mu_s}{b_a^3} \mathbf{r}_s^I + 3 \frac{\mu_s}{b_a^5} \left((\mathbf{r}_s^I)^T \mathbf{b}_a^I \right) \mathbf{b}_a^I + \mathbf{C}_{sI}^T \frac{\partial V_{po}}{\partial \mathbf{r}_s^I} \quad (78)$$

- Rigid body spacecraft relative dynamics under spherical harmonics gravitation (up to second degree-and-order),

$$m_s \ddot{\mathbf{r}}_s^I \approx \left[-m_s \left(\frac{\mu_s}{b_a^3} + \frac{\mu_a}{r_s^3} \right) + \frac{15}{2} \left(\frac{\mu_a ((\mathbf{r}_s^I)^T \mathbf{I}_s^I (\mathbf{r}_s^I))}{r_s^7} \right) \right] \mathbf{r}_s^I - 3 \left(\frac{\mu_a}{r_s^5} \right) \boldsymbol{\varXi} \mathbf{r}_s^I + 3 m_s \frac{\mu_s}{b_a^5} (\mathbf{r}_s^I \mathbf{b}_a^I) \mathbf{b}_a^I + \mathbf{C}_{sI}^T \mathbf{F}_{ga2}^s \quad (79)$$

- Rigid body spacecraft relative dynamics under polyhedron augmented gravitation,

$$\ddot{\mathbf{r}}_s^I \approx -\frac{\mu_s}{b_a^3} \mathbf{r}_s^I + 3 \frac{\mu_s}{b_a^5} ((\mathbf{r}_s^I)^T \mathbf{b}_a^I) \mathbf{b}_a^I + \mathbf{C}_{sI}^T \frac{\partial V_{po}}{\partial \mathbf{r}_s^I} + \frac{1}{m_s} \left(\sum_{i=1}^N \mathbf{C}_{Ip_i} (\mathbf{f}_{g2_i}^p + \mathbf{f}_{g4_i}^p) \right) \quad (80)$$

Comparing both sides of Eq. (77) during a numerical simulation shows that the error stays below the order of $\pm 2 \times 10^{-15}$. This is an order of significance higher than the machine epsilon for double precision floating-point format (2.22×10^{-16}), therefore we consider the approximation performed to be good enough for our purposes in this paper.

The above equations were implemented in Fortran, and the numerical integrator used was a Runge-Kutta 4th order (RK4) single step method. The time-step used for all simulations was 0.25 s. Numerical results were then imported to MATLAB for data analysis and plotting. Additionally, a collision detection script was implemented in the numerical integrator algorithm in Fortran for both polyhedron gravitational models, to detect possible impacts with the asteroid's surface during simulation runtime. The spacecraft quaternion normalization error was kept below $\pm 5 \times 10^{-16}$ (close to two times the machine epsilon) during the whole integration interval.

Individual spacecraft trajectories will be shown relative to the asteroid, in an orbiting frame fixed at the center of mass of the asteroid, with one axis pointing towards the Sun, another one pointing perpendicular to the orbital plane, and the third one completing the orthogonal triad pointing towards the asteroid's direction of motion. In addition, to compare gravitational models in a representative way, and to plot the position error between different models, a *relative dynamics reference frame* is implemented. This relative frame is similar to the frame used in studying spacecraft formation flying, known as *Hill Frame*.³³ It is centered on the *leader* spacecraft, and is named \mathcal{F}_R , with axes defined as

$$\begin{aligned} \hat{\mathbf{x}}_R &= \frac{\dot{\mathbf{r}}_{s_l}^I}{\|\dot{\mathbf{r}}_{s_l}^I\|} \\ \hat{\mathbf{y}}_R &= \frac{\mathbf{r}_{s_l}^I \times \dot{\mathbf{r}}_{s_l}^I}{\|\mathbf{r}_{s_l}^I \times \dot{\mathbf{r}}_{s_l}^I\|} \\ \hat{\mathbf{z}}_R &= \frac{\hat{\mathbf{x}}_R \times \hat{\mathbf{y}}_R}{\|\hat{\mathbf{x}}_R \times \hat{\mathbf{y}}_R\|} \end{aligned} \quad (81)$$

where $\mathbf{r}_{s_l}^I$ is the *leader* spacecraft (i.e. spacecraft reference model) relative position with respect to the asteroid, resolved in the inertial frame. The associated rotation matrix \mathbf{C}_{RI} can be formed via the basis vectors from Eq. (81). Then, a relative position vector can be defined in the inertial frame as $\boldsymbol{\rho}^I = \mathbf{r}_{s_f}^I - \mathbf{r}_{s_l}^I$, with \mathbf{r}_{s_f} being the relative position of the *follower* spacecraft with respect to the asteroid. Expressing this relative position vector in the reference frame \mathcal{F}_R with the help of \mathbf{C}_{RI} , results in $\boldsymbol{\rho}^R = \mathbf{C}_{RI} \boldsymbol{\rho}^I$. This approach allows direct comparison between spacecraft models (e.g. rigid body spacecraft under the spherical harmonics and polyhedron gravitational models), by plotting relative deviations of the spacecraft under one gravitational model against another, as a function of time. These deviations can be observed in the different components of $\boldsymbol{\rho}^R$, that are identified as the *along-track component*, the *out-of-plane component*, and the *quasi-radial component* respectively.

B. Spacecraft parameters

For numerical simulations, the selected physical parameters for the spacecraft are shown in table 1. The size and mass of the spacecraft selected are representative of actual missions to small bodies such as JAXA’s Hayabusa mission to asteroid 25143 Itokawa³¹ and ESA’s Rosetta mission to comet 67P/Churyumov–Gerasimenko.³²

Table 1. Spacecraft parameters

Size [m]		Moments of inertia				
Zeroth Order [kg]	Second Order [$\times 10^{-3}$ kg km ²]	Fourth Order [$\times 10^{-9}$ kg km ⁴]				
$h = 2.1$	$m_s = 3000$	$I_{xx} = 3.0625$	$I_{xxxx} = 4.4748$	$I_{yyxx} = 3.8498$	$I_{zzxx} = 0.4127$	$I_{xyyx} = 0.3675$
$w = 2.0$		$I_{yy} = 2.96$	$I_{xxyy} = 4.2423$	$I_{yyyy} = 4.2116$	$I_{zzyy} = 0.4796$	$I_{xzzx} = 0.6533$
$t = 2.8$		$I_{zz} = 2.1025$	$I_{xxzz} = 4.5281$	$I_{yyzz} = 4.2026$	$I_{zzzz} = 2.0643$	$I_{yzzy} = 0.7203$

C. Simulation results

1. Trajectories about 433 Eros

In this section, a simulation is presented for asteroid 433 Eros, where the spacecraft trajectories lie outside the Brillouin sphere. Eros initial position is assumed at perihelion, rotating about its maximum moment of inertia axis. Physical, orbital and attitude parameters for Eros are presented in table 2. The shape model was filled with 7574 point-masses uniformly distributed in a grid, resulting in a three dimensional resolution of 693.52 m. As the asteroid attitude motion is common to all gravitational models, it does not affect the comparison between them. In order to make a more fair comparison between gravitational models, sectorial harmonics were calculated for the shape model filled with point-masses, and normalized via the radius r_o . This reflects more accurately the particular shape of the asteroid, and the point-mass distribution inside the shape. Initial conditions for the spacecraft relative to the asteroid, expressed in the inertial frame \mathcal{F}_I , are shown in table 3.

The simulation was performed for a trajectory lasting 22 days. Figure 6 presents trajectories and relative error for a rigid body spacecraft, calculated using both the expanded polyhedron and spherical harmonics gravitational models. The asteroid is shown in its final orientation at the end of the simulation. For the relative position error plots, the rigid body spacecraft under the augmented polyhedron gravitational model is chosen to be the *leader*, and the rigid body spacecraft under the spherical harmonics model is selected as the *follower*. It is clear that there are large deviations between the polyhedron and the spherical harmonics gravitational models, despite the fact that both trajectories lie outside (but very close) to the Brillouin sphere. The difference between trajectories of the point-mass compared to the rigid body spacecraft due to orbital-attitude coupling becomes evident, as shown in figure 7 for the proposed expanded polyhedron model. In this scenario, the point-mass trajectory is chosen to be the *leader*, while the rigid body is the *follower* (i.e. $\rho^I = \mathbf{r}_{s_{RB}}^I - \mathbf{r}_{s_{PM}}^I$).

2. Trajectories about 4769 Castalia

Another simulation is presented about asteroid 4769 Castalia. This time, trajectories for 6 days are simulated, starting outside the Brillouin sphere. Spacecraft parameters are once again those given in table 1. Similarly to Eros, physical, orbital and rotational parameters for Castalia are shown in table 4. For this asteroid, 3285 point-masses were uniformly distributed in a grid inside the asteroid’s shape model, giving a resolution of 58.74 m. As with Eros, sectorial harmonics C_2^0 and C_2^2 were calculated for the shape model filled with point-masses, and normalized via the radius r_o , to better reflect the shape and point-masses distribution inside this asteroid. Additionally, table 5 shows the spacecraft initial values relative to the asteroid, in the inertial frame \mathcal{F}_I .

Table 2. Parameters for 433 Eros

Parameter	Symbol	Value	Units
Mass ³⁴	M	6.69×10^{15}	[kg]
Rotation Period ¹	—	5.2702	[h]
Eccentricity ³⁵	e	0.22268	—
Perihelion ³⁵	q	1.13324	[AU]
Inclination ³⁵	i	10.82860	[°]
Long. of Ascending Node ³⁵	Ω	304.32982	[°]
Argument of Perihelion ³⁵	ω	178.79804	[°]
Pole Ecliptic Long. (J2000) ¹	λ	17.23085	[°]
Pole Ecliptic Lat. (J2000) ¹	β	11.36299	[°]
Sectorial Harmonic	C_2^0	-0.09699	—
Sectorial Harmonic	C_2^2	0.04402	—
Normalizing radius	r_o	17.68477	[km]
	e_1	-0.51628	—
Initial attitude	e_2	-0.36734	—
quaternion in \mathcal{F}_I	e_3	0.60419	—
	e_0	-0.48317	—

Table 3. Initial spacecraft conditions relative to 433 Eros

Position [km]	Velocity [km/s]	Attitude Quat.	Ang. Velocity [rad/s]
[0 25 0]	[0 0 0.005]	[0 0 0 1]	[0.002 0.001 0.003]

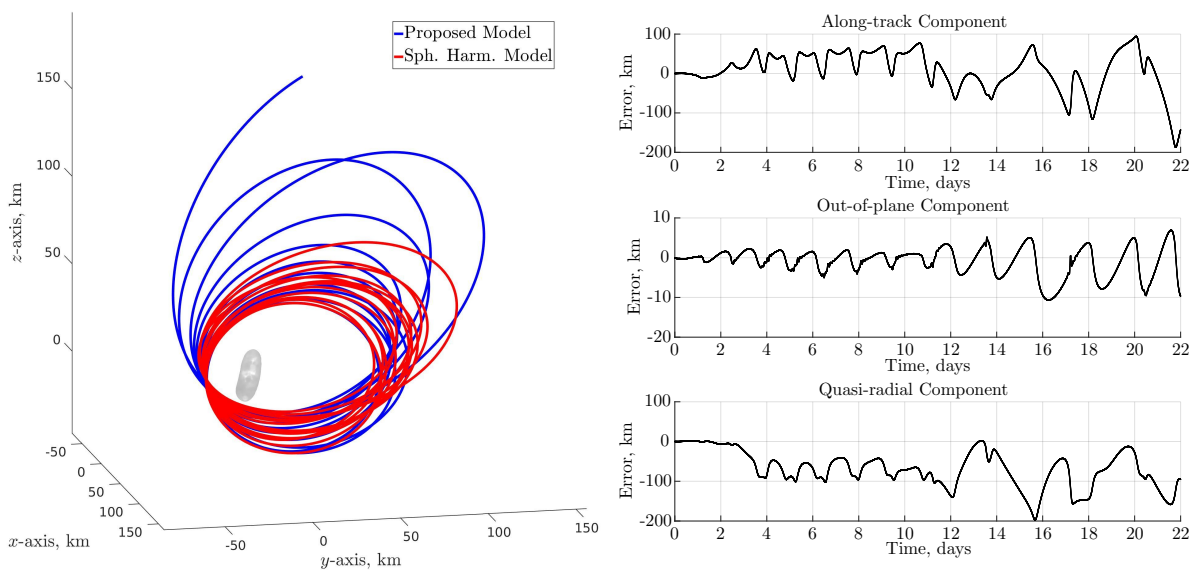


Figure 6. Rigid body spacecraft trajectories and relative errors for 22 days about 433 Eros

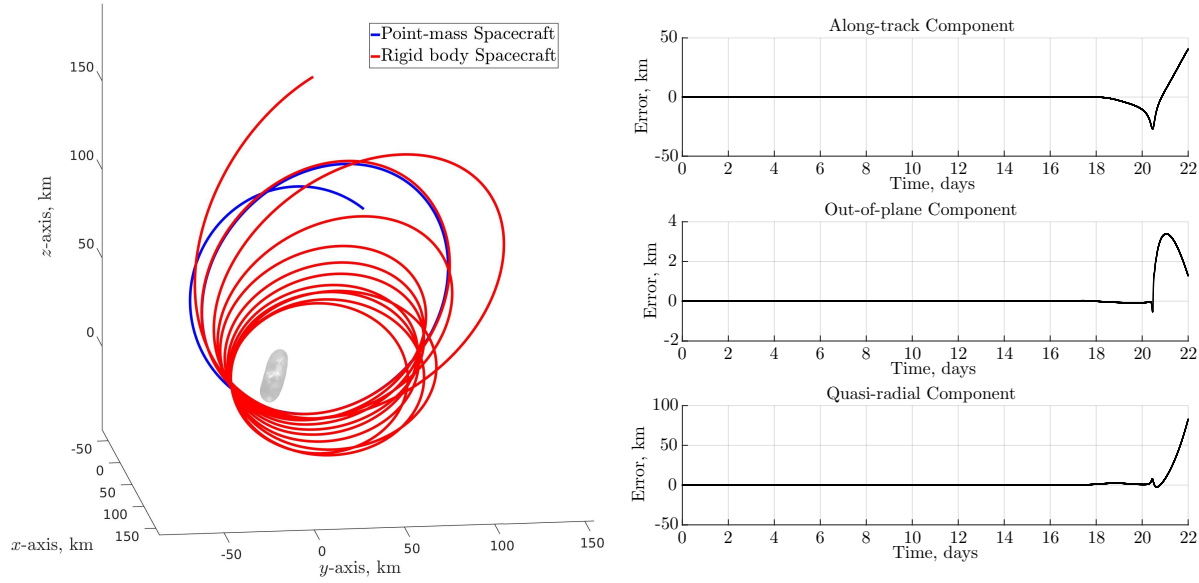


Figure 7. Point-mass and rigid body spacecraft trajectories and relative errors for 22 days about 433 Eros (Expanded polyhedron model)

Table 4. Parameters for 4769 Castalia

Parameter	Symbol	Value	Units
Mass ¹⁴	M	1.41×10^{15}	[kg]
Rotation Period ³⁶	—	4.095	[h]
Eccentricity ³⁵	e	0.48313	—
Perihelion ³⁵	q	0.54957	[AU]
Inclination ³⁵	i	8.88626	[°]
Long. of Ascending Node ³⁵	Ω	325.59192	[°]
Argument of Perihelion ³⁵	ω	121.35334	[°]
Pole Ecliptic Long. (J2000) ³⁶	λ	253.00	[°]
Pole Ecliptic Lat. (J2000) ³⁶	β	56.00	[°]
Sectorial Harmonic	C_2^0	-0.08886	—
Sectorial Harmonic	C_2^2	0.03651	—
Normalizing radius	r_o	0.88111	[km]
	e_1	0.14333	—
Initial attitude	e_2	-0.25483	—
quaternion in \mathcal{F}_I	e_3	-0.65959	—
	e_0	0.69243	—

Table 5. Initial spacecraft conditions relative to 4769 Castalia

Position [km]	Velocity [km/s]	Attitude Quat.	Ang. Velocity [rad/s]
[0 0.9 0]	[0 0 0.00042]	[0 0 0 1]	[0.0025 0 0.007]

For this case, the initial position of the spacecraft is on the terminator plane. Trajectories for the rigid body spacecraft calculated via both gravitational models together with their relative errors are shown in figure 8. Both trajectories enter the Brillouin sphere. Similar to Eros, there is a noticeable difference between spacecraft trajectories corresponding to each gravitational model. The asteroid attitude shown is the one presented by the asteroid at the end of the simulation, as previously done for Eros. Figure 9 presents a comparison between point-mass and rigid body spacecraft trajectories for the polyhedron model, sided by the relative position error between both spacecraft models. Once again, the point-mass spacecraft is used as the leader trajectory for comparison with the rigid body spacecraft. As with the trajectories for Eros, a large deviation is noticed between the point-mass and the rigid body trajectory. This highlights once again the effect that spacecraft attitude variations have on the orbital motion during close proximity to the asteroid.

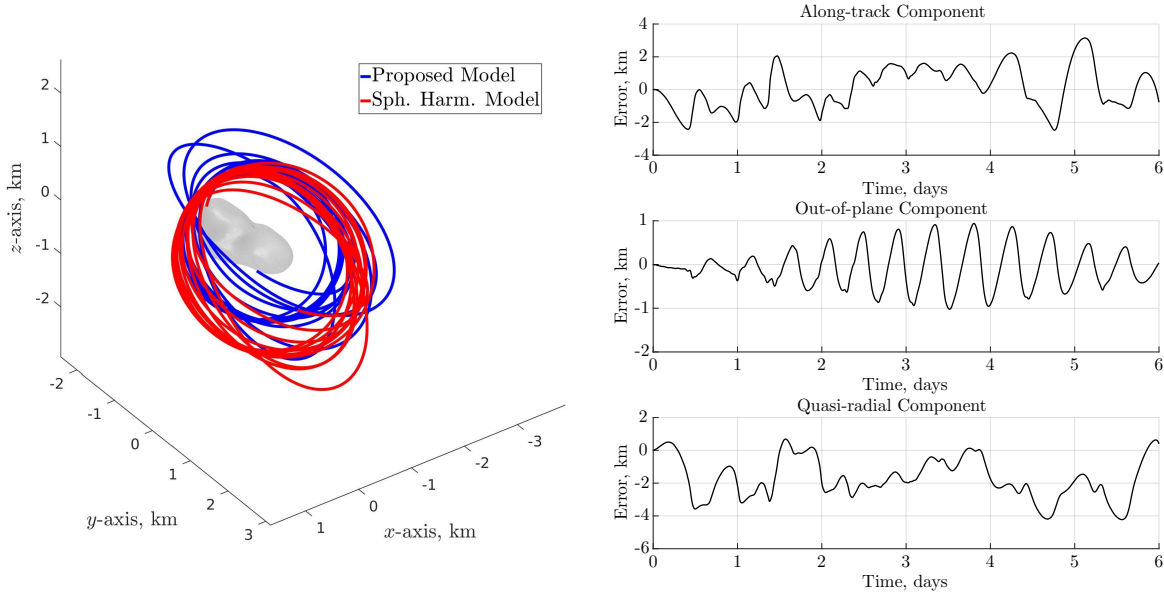


Figure 8. Rigid body spacecraft trajectories and relative errors for 6 days about 4769 Castalia

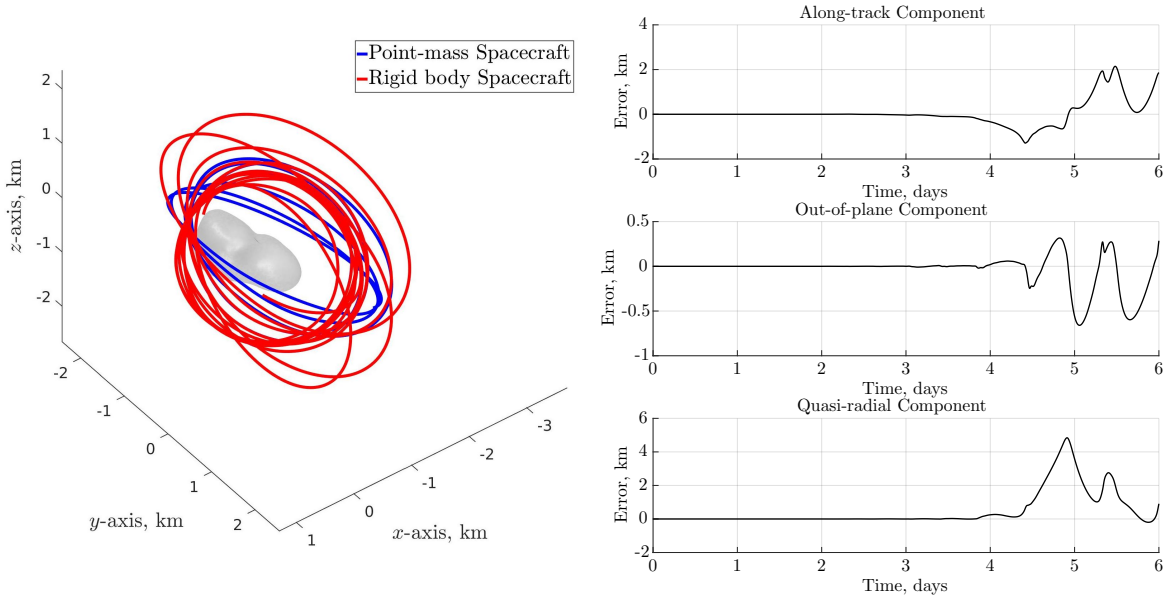


Figure 9. Point-mass and rigid body spacecraft trajectories and relative errors for 6 days about 4769 Castalia (Expanded polyhedron model)

Figure 10 shows the relative position error between the full augmented polyhedron model against the same model considering terms up to second order, for a rigid body spacecraft orbiting Castalia, using the same initial values as depicted in table 5. The same *leader - follower* approach used before was applied for this plot, considering the full model the *leader* trajectory, and the gravitational model including terms up to $\mathcal{O}(\varepsilon^2)$ as the *follower*. This figure clearly shows the effect of the inclusion of the $\mathcal{O}(\varepsilon^4)$ terms in the gravitational force and torque expansions for a rigid body spacecraft. As previously mentioned in Section IV before introducing the expanded polyhedron model, the inclusion of coupling terms above $\mathcal{O}(\varepsilon^4)$ becomes unnecessary, since their calculation growths in complexity while contributing less than the $\mathcal{O}(\varepsilon^4)$ terms. Even if these terms were developed and included, it would introduce a very high computational demand, as demonstrated by the complex equations for the higher order force and torque terms up to the fourth order (Eqs. (63) to (65), and Eqs. (73) to (75)).

D. Numerical integrator error considerations

On numerical integration Runge-Kutta methods, two errors are involved: the *round-off* error, and the *truncation* error.³⁷ Round-off error is due to the finite precision numerical representation used by the computer in calculations (in this case double-precision floating point), and since it depends on the type and number of arithmetic operations performed at each step, together with the type of computer that is used, its calculation typically becomes a very difficult task. Thus it will not be considered in this analysis. We are mostly interested in the truncation errors, which are the *local truncation error* (LTE) and the *global truncation error* (GTE). The LTE is the error introduced at each integration step, and the GTE is the cumulative truncation error at the end of the integration interval. Hence, it is of interest to compute the GTE for the state vector.

At the end of the integration interval (t_0, t) , the GTE can be calculated as³⁸

$$E(y(t), h) = |y(t) - y^*(t)| = \mathcal{O}(h^4) \quad (82)$$

where h is the integration step, $y(t)$ is the exact solution at time t , and $y^*(t)$ is the estimation due to the RK4 method at time t . Equation (82) shows that the GTE is proportional to $\mathcal{O}(h^4)$. Then, this error can be approximated by³⁸

$$E(y(t), h) \approx Kh^4 \quad (83)$$

where K is a constant that is assumed not to change as t varies. As the exact solution $y(t)$ is not known, the constant K is unknown. However, it can be estimated via two approximations: one with a time-step h , and another one with time-step $h/2$. Therefore

$$\begin{aligned} E(y(t), h/2) - E(y(t), h) &= |y^*(t, h) - y^*(t, h/2)| \\ &= Kh^4 \left(\left(\frac{1}{2} \right)^4 - 1 \right) \end{aligned} \quad (84)$$

Then³⁸

$$K = \frac{|y^*(t, h) - y^*(t, h/2)|}{h^4 \left(\left(\frac{1}{2} \right)^4 - 1 \right)} \quad (85)$$

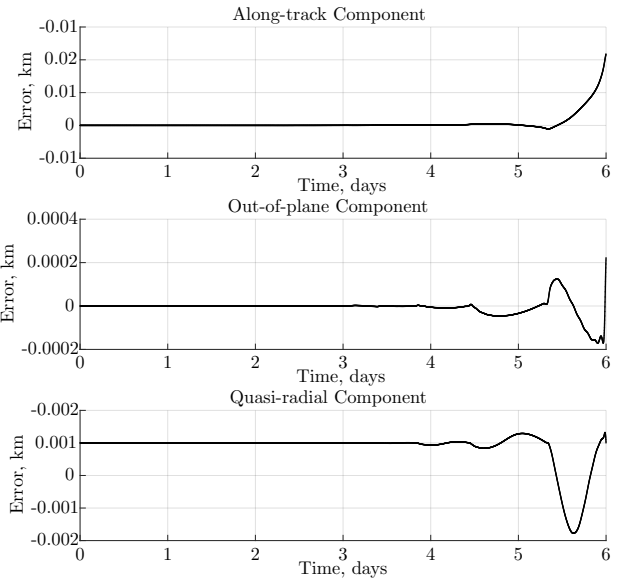


Figure 10. Difference between full gravitational model versus same model including terms up to second order

With K approximated as in Eq. (85), the GTE for a given time-step can then be calculated. Of course, it is necessary to obtain the state vector at the end of two simulations to be able to approximate this constant, but a measure of the GTE via this method gives a good idea on the numerical errors at the end of the integration interval.

For the simulations performed in this study, the selected time-steps for computing the GTE where $h = 0.5$ s and $h/2 = 0.25$ s. Table 6 shows the largest GTE percentage presented by any given component of the position, velocity, quaternion and angular velocity values of the spacecraft at the end of the simulations, using the polyhedron gravitational models for the asteroid.

Table 6. Percentage GTE for numerical simulations (Polyhedron gravitational models)

Asteroid	Spacecraft Model	GTE			
		Position [%]	Velocity [%]	Attitude Quat. [%]	Ang. Velocity [%]
433 Eros	Point-mass	1.5318×10^{-1}	3.3120×10^{-1}	—	—
	Rigid body	3.0685×10^{-1}	2.5863×10^{-2}	5.8810×10^{-2}	1.4064×10^{-4}
4769 Castalia	Point-mass	3.8083×10^{-4}	3.1763×10^{-4}	—	—
	Rigid-body	4.2315×10^{-4}	6.3893×10^{-5}	3.2195×10^{-6}	6.6701×10^{-6}

These values show that the truncation error introduced by the RK4 integrator as configured for the simulations is acceptable for the time frames of the trajectories previously presented.

VI. Conclusion

An expansion of the polyhedron model with point-masses filling the entire shape model was proposed to account for the orbit-attitude coupling phenomena (up to the second order) of a rigid body spacecraft. This gravitational model was then compared to a spherical harmonics model used in the current literature, that is expanded up to second-degree-and-order and also considers orbit-attitude coupling (up to the first order). It was shown that with the proposed high fidelity gravitational model, the spacecraft attitude motion has a significant effect on the spacecraft orbital motion, as has previously been observed with the spherical harmonics gravitational model. However, as demonstrated in this paper, there is also a significant difference of the spacecraft orbital motion between the proposed high fidelity model and the spherical harmonics model. This indicates that the spherical harmonics model may not be sufficient for mission planning, nor for developing control laws that exploit the orbit-attitude coupling, particularly when the spacecraft is in close proximity to the asteroid.

Acknowledgments

This research was partially funded by the Natural Sciences and Engineering Research Council of Canada.

References

- ¹Miller, J. K., Konopliv, A. S., Antreasian, P. G., Bordi, J. J., Chesley, S., Helffrich, C. E., Owen, W. M., Wang, T. C., Williams, B. G., and Yeomans, D. K., "Determination of Shape, Gravity, and Rotational State of Asteroid 433 Eros," *Icarus*, Vol. 155, No. 1, 2002, pp. 3–17.
- ²Scheeres, D., Gaskell, R., Abe, S., Barnouin-Jha, O., Hashimoto, T., Kawaguchi, J., Kubota, T., Saito, J., Yoshikawa, M., Hirata, N., Mukai, T., Ishiguro, M., Kominato, T., Shirakawa, K., and Uo, M., "The Actual Dynamical Environment About Itokawa," *AIAA/AAS Astrodynamics Specialist Conference and Exhibit*, edited by AIAA/AAS, August 2006.
- ³Scheeres, D., *Orbital Motion In Strongly Perturbed Environments*, Springer-Praxis, Berlin, Germany, 1st ed., 2012.
- ⁴Schaub, H. and Junkins, J. L., *Analytical Mechanics of Space Systems*, AIAA, Inc., 3rd ed., 2014.
- ⁵Sincarsin, G. B., *Gravitational Orbit-Attitude Coupling and Penumbra-Gradient Torques for Very Large Spacecraft*, Phd dissertation, University of Toronto - Institute for Aerospace Studies, November 1982.
- ⁶Hughes, P. C., *Spacecraft Attitude Dynamics*, Dover Publications, Inc., Mineola, NY, USA, dover edition ed., 2004.
- ⁷JAXA, "Asteroid Explorer "Hayabusa-2," <http://www.jspec.jaxa.jp/e/activity/hayabusa2.html>, Retrieved on January 12, 2016.

⁸NASA, "OSIRIS-REx Website," https://www.nasa.gov/mission_pages/osiris-rex/index.html, Retrieved on January 12, 2016.

⁹Mazanek, D. D., Merrill, R. G., Brophy, J. R., and Mueller, R. P., "Asteroid Redirect Mission concept: A bold approach for utilizing space resources," *Acta Astronautica*, Vol. 117, Dec 2015, pp. 163–171.

¹⁰Misra, G., Sanyal, A., and Samiei, E., "Asteroid Landing Guidance Design in the Framework of Coupled Orbit-Attitude Spacecraft Dynamics," *AAS 5-430 Conference Paper*, 2015.

¹¹Werner, R. A. and Scheeres, D., "Exterior Gravitation of a Polyhedron Derived and Compared with Harmonic and Mascon Gravitation Representations of Asteroid 4769 Castalia," *Celestial Mechanics and Dynamical Astronomy*, Vol. 65, No. 3, 1997, pp. 313–344.

¹²Scheeres, D. J., "Dynamics about uniformly rotating triaxial ellipsoids: Application to asteroids," *Icarus*, Vol. 110, No. 2, 1994, pp. 225 – 238.

¹³Scheeres, D. J., "Orbit Mechanics About Asteroids and Comets," *Journal of Guidance, Control and Dynamics*, Vol. 35, No. 3, May-June 2012, pp. 987 – 997.

¹⁴Scheeres, D., Ostro, S. J., Hudson, R. S., and Werner, R. A., "Orbits Close to Asteroid 4769 Castalia," *Icarus*, Vol. 121, No. 0072, 1996, pp. 67–87.

¹⁵Hu, W., *Orbital Motion in Uniformly Rotating Second Degree and Order Gravity Fields*, Phd dissertation, University of Michigan, Ann Arbor, MI, USA, 2002.

¹⁶Kumar, K. D., "Attitude dynamics and control of satellites orbiting rotating asteroids," *Acta Mechanica*, Vol. 198, No. 1-2, 2008, pp. 99–118.

¹⁷Wang, Y. and Xu, S., "Gravitational Orbit-Rotation Coupling of a Rigid Satellite around a Spheroid Planet," *Journal of Aerospace Engineering*, Vol. 27, No. 1, January 2014, pp. 140 – 150.

¹⁸Misra, G. and Sanyal, A., "Analysis of Orbit-Attitude Coupling of Spacecraft Near Small Bodies," *AIAA Conference Paper*, 2015.

¹⁹Misra, G., Maziar, I., Sanyal, A., and Scheeres, D., "Coupled Orbit-Attitude Dynamics and Relative State Estimation of Spacecraft Near Small Solar System Bodies," *Advances in Space Research*, Vol. 57, No. 8, April 2016, pp. 1747–1761.

²⁰Lantoine, G., *Optimal trajectories for soft landing on asteroids*, Special Problems Report, Space Systems Design Lab (SSDL), School of Aerospace Engineering, Georgia Institute of Technology, Atlanta, GA, December 2006.

²¹Park, R. S., Werner, R. A., and Bashkaran, S., "Estimating Small-Body Gravity Field from Shape Model and Navigation Data," *Journal of Guidance, Control and Dynamics*, Vol. 33, No. 1, January - February 2010, pp. 212–221.

²²Yu, Y. and He-xi, B., "Routing the asteroid surface vehicle with detailed mechanics," *Acta Mechanica Sinica*, Vol. 30, No. 3, February 2014, pp. 301–309.

²³Muller, P. M. and Sjogren, W. L., "Mascon: Lunar Mass Concentrations," *Science*, Vol. 161, No. 3842, August 1968, pp. 680–684.

²⁴Sjogren, W., Muller, P., Gottlieb, P., Wong, L., Buecheler, G., Downs, W., and Prislin, R., "Lunar Surface Mass Distribution From Dynamical Point-Mass Solution," *The Moon*, Vol. 2, No. 3, 1971, pp. 338–353.

²⁵Geissler, P., Petit, J. M., Durda, D. D., Greenberg, R., Bottke, W., Nolan, M., and Moore, J., "Erosion and Ejecta Reaccretion on 243 Ida and its Moon," *Icarus*, Vol. 120, No. 1, 1996, pp. 140–157.

²⁶Ashenberg, J., "Proposed Method for Modeling the Gravitational Interaction Between Finite Bodies," *Journal of Guidance, Control and Dynamics*, Vol. 28, No. 4, July-August 2005, pp. 768–774.

²⁷Russell, R. P. and Arora, N., "Global Point Mascon Models for Simple, Accurate, and Parallel Geopotential Computation," *Journal of Guidance, Control and Dynamics*, Vol. 35, No. 5, September - October 2012, pp. 1568 – 1581.

²⁸Maruya, M., Ohyama, H., Masashi, U., Muranaka, N., Morita, H., Kubota, T., Hashimoto, T., Saito, J., and Kawaguchi, J., "Navigation Shape and Surface Topography Model of Itokawa," *AIAA/AAS Astrodynamics Specialist Conference and Exhibit*, 2006.

²⁹Sincarsin, G. B. and Hughes, P. C., "Gravitational orbit-attitude coupling for very large spacecraft." *Celestial mechanics*, Vol. 31, No. 2, May 1983, pp. 143–161.

³⁰NASA, "NASA Planetary Data System - PDS Asteroid/Dust Archive - Shape Model," <http://sbn.psi.edu/pds/archive/shape.html>, Retrieved on May, 2015.

³¹JAXA, "Asteroid Explorer "Hayabusa" (MUSES-C)," http://global.jaxa.jp/projects/sat/muses_c/, Retrieved on February 18, 2016.

³²ESA, "The Rosetta Orbiter," http://www.esa.int/Our_Activities/Space_Science/Rosetta/The_Rosetta_orbiter, 2014, Retrieved on February 18, 2016.

³³de Ruiter, A. H., Damaren, C., and Forbes, J. R., *Spacecraft Dynamics and Control: An Introduction*, John Wiley & Sons, Ltd., West Sussex, UK, 1st ed., 2013.

³⁴Carry, B., "Density of Asteroids," *Planetary and Space Science*, Vol. 73, No. 1, 2012, pp. 98 – 118.

³⁵JPL, "JPL Small-Body Database Browser," <http://ssd.jpl.nasa.gov/sbdb.cgi>, Retrieved on February 15, 2016.

³⁶Hudson, R. S., Ostro, S. J., and Harris, A. W., "Constraints on Spin State and Hapke Parameters of Asteroid 4769 Castalia Using Lightcurves and a Radar-Derived Shape Model," *Icarus*, Vol. 130, No. 1, Nov 1997, pp. 165–176.

³⁷Cartwright, J. H. E. and Piro, O., "The Dynamics of the Runge-Kutta Methods," *International Journal of Bifurcation and Chaos*, Vol. 2, No. 03, September 1992, pp. 427–449.

³⁸Mathews, J. H. and Fink, K. K., *Numerical Methods Using Matlab*, Pearson, Upper Saddle River, NJ, USA, 4th ed., 2004.